universität wien

MASTERARBEIT / MASTER'S THESIS

Titel der Masterarbeit / Title of the Master's Thesis

„ Accurate characterization of β-Amyloid (Aβ40, Aβ42) standards using species-specific HPLC-ICP-MS/MS “

verfasst von / submitted by

Martin Schaier BSc

angestrebter akademischer Grad / in partial fulfilment of the requirements for the degree of

Master of Science (MSc)

Wien, 2020 / Vienna 2020

Studienkennzahl lt. Studienblatt / degree programme code as it appears on the student record sheet:	A >066 862<
Studienrichtung lt. Studienblatt / degree programme as it appears on the student record sheet:	Master Chemie
Betreut von / Supervisor:	Univ.-Prof. Dr. Gunda Köllensperger

Acknowledgments

First, I would like to thank Gunda Köllensperger for the opportunity to work in her research group in the last years. This enabled me to gain a lot of important experience that I would otherwise not have been able to do. I also really appreciate that my personal interests were addressed in writing my master's thesis in the field of Alzheimer's research.

Furthermore, I would like to thank all my colleagues for providing such a great atmosphere in the working group. Regular activities such as hiking, soccer or drinking together made everyday life really varied and fun. The daily lunch with everyone, where nobody can decide what to eat, has also found a new meaning for me.

I would particularly like to thank Evelyn Rampler for always listening to my concerns and helping me with sample preparation, especially since I had no direct practical supervisor. My sincere thanks also go to Luis Galvez for explaining the HPLC to me in such detail and for always being available if I had any problems, even though he was busy with his doctoral thesis himself. I am also grateful to Gerrit Herrmann for providing me with his excellent yeast standards, which made this work possible.

Special thanks go to Sophie Neumayer and Sarah Theiner, who were helping me a lot over the years with ICP-MS and organizational stuff.

Finally, I would like to thank my friends and family sincerely for their continued support. Regularly visiting home has always given me great joy and helped me to relieve myself from stressful times.

This thesis received funding by the European ReMiND project (nr: 15HLT02).

Contents

List of abbreviations

Aβ	Amyloid β peptide
Aβ40	β-Amyloid peptide fragment 1-40
Aβ42	β-Amyloid peptide fragment 1-42
ACN	Acetonitrile
AD	Alzheimer´s disease
APP	Amyloid β precursor protein
Ar	Argon
As	Arsenic
BEH	Bridged ethylene hybrid
CAS	Chemical abstract service
CE	Capillary electrophoresis
CPS	Counts per second
Cr	Chromium
CRC	Collision/reaction cell
CSF	Cerebrospinal fluid
DEAE	Diethyl-aminoethyl
ESA	Electrostatic analyser
ESI-MS	Electrospray ionization mass spectrometry
Fe	Iron
GSSG	Glutathione disulfide
H_2	Hydrogen
H_2O	Water

H_2O_2	Hydrogen peroxide
HAc	Acetic acid
HCl	Hydrochloric acid
Hg	Mercury
HMW	High molecular weight
HPLC	High performance liquid chromatography
HSA	Human serum albumin
GC	Gas chromatography
ICP-MS/MS	Inductively coupled plasma triple quadrupole mass spectrometry
IDMS	Isotope dilution mass spectrometry
IPA	Isopropanol
LMW	Low molecular weight
LOD	Limit of detection
LOQ	Limit quantification
m/z	Mass to charge ratio
MeOH	Methanol
N/A	Not available
NH_3	Ammonia
NH_4Ac	Ammonia acetate
NH_4OH	Ammonia hydroxide
O_2	Oxygen
PET	Positron emission tomography
PEEK	Polyetheretherketone

PFA	Perfluoroalkoxy alkane
QQQ	Triple quadrupole mass spectrometer
rcf	Relative centrifugal force
ReTOF	Reflectron time-of-flight mass spectrometry
RF	Radio frequency
RIDMS	Reverse isotope dilution mass spectrometry
ROS	Reactive oxygen species
RSQ	R-squared
RT	Retention time
r.t.	Room temperature
S	Sulfur
SAX	Strong anion exchange
Se	Selenium
SEC	Size exclusion chromatography
SEM	Secondary electron multiplier
SF	Sector field
SQ	Single quadrupole
SRM	Standard reference material
TOF	Time-of-flight
TRA	Time resolved analysis
WHO	World health organization

Abstract[1]

One of the greatest challenges in medicine today is the fight against neurodegenerative diseases such as Alzheimer's disease. A defining pathological feature is the formation of plaques in the extracellular regions of the brain with the β-Amyloid (Aβ40, Aβ42) peptide being the main component of this deposit. Therefore, the study of this peptide gives the opportunity to get a better insight into the processes of this complex disease.

For clinical analysis one needs suitable standards, but it is not an easy task to find them, since only a few are commercially available, and these vary in their purity. Furthermore, the determination of absolute concentration in most protein standards is performed in a non-traceable manner, by e.g. Bradford assay in which albumin is used as a calibrant. Hence, accurate methods are needed to characterize these standards.

The aim of this study was to quantify synthetic β-Amyloid standards (purchased from r-Peptide) by analysing the sulfur-content of its amino acids. For this purpose, an acid-hydrolysis of the peptide was performed. The so obtained individual amino acids were separated by means of a strong anion exchange column and directly analysed with inductively coupled plasma mass spectrometry (ICP-MS/MS) in oxygen mode. Species-specific isotope dilution was applied using an ^{34}S-enriched yeast hydrolysate to correct for potential losses within sample preparation. In order to validate the established method in an appropriate manner for the amino acids, methionine and cysteine, a standard reference material (NIST 2389a) was used. In addition, the commercially available proteins lysozyme and myoglobin were successfully quantified by this procedure. Measuring the whole protein and peptide standards via size exclusion chromatography allowed further characterization of their purity. To prevent sulfur contamination, all consumables were pre-cleaned with nitric acid. Ultimately the combination of HPLC-ICP-MS/MS with species-specific ID allowed us to accurately quantify β-Amyloid standards with high throughput and low volume consumption.

[1] This abstract was published in a conference proceeding with the title: Accurate quantification of β-amyloid standards through sulfur on-line isotope dilution using LC-ICP-MS/MS, poster presentation, ReMIND 2019 Biomolecules in Neurodegenerative Diseases, Physikalisch-Technische Bundesanstalt, Braunschweig, Germany, 26-27.06.2019

Zusammenfassung

Eine der größten Herausforderungen in der heutigen Medizin ist der Kampf gegen neurodegenerative Erkrankungen wie die Alzheimer-Krankheit. Ein entscheidendes pathologisches Merkmal ist die Bildung von Plaques in den extrazellulären Regionen des Gehirns, wobei das β-Amyloid (Aβ40, Aβ42)-Peptid den Hauptbestandteil dieser Ablagerungen darstellt. Daher bietet die Untersuchung dieses Peptids die Möglichkeit, einen besseren Einblick in die Prozesse einer so komplexen Krankheit zu erhalten.

Für die klinische Analyse werden hierfür geeignete Standards benötigt, welche jedoch nicht leicht zu finden sind, da nur wenige kommerziell erhältlich sind und diese oft in ihrer Reinheit variieren. Weiterhin wird die Bestimmung der absoluten Konzentration für die meisten Proteinstandards auf nicht rückverfolgbare Weise durchgeführt, z.B. mittels Bradford-Assay, bei welchem Albumin für die Kalibration herangezogen wird. Daher sind genauere Methoden erforderlich, um diese Standards zu charakterisieren.

Ziel dieser Studie war es, synthetische β-Amyloid-Standards (bezogen von r-Peptide) durch Analyse des Schwefelgehalts ihrer Aminosäuren zu quantifizieren. Zu diesem Zweck wurde eine Säurehydrolyse des Peptids durchgeführt. Die so erhaltenen einzelnen Aminosäuren wurden mittels einer starken Anionenaustauschersäule aufgetrennt und direkt über Massenspektrometrie mit induktiv gekoppeltem Plasma (ICP-MS/MS) im Sauerstoffmodus analysiert. Speziesspezifische Isotopenverdünnung wurde unter Verwendung eines ^{34}S-angereicherten Hefehydrolysats angewandt, um mögliche Verluste bei der Probenvorbereitung zu korrigieren. Um die etablierte Methode in geeigneter Weise für die Aminosäuren Methionin und Cystein zu validieren, wurde ein Standard-Referenzmaterial (NIST 2389a) verwendet. Zusätzlich wurden die kommerziell erhältlichen Proteine Lysozym und Myoglobin durch dieses Verfahren erfolgreich quantifiziert. Die Messung der ganzen Protein- und Peptidstandards mittels Größenausschlusschromatographie ermöglichte eine weitere Charakterisierung ihrer Reinheit. Um dabei Kontaminationen mit Schwefel zu vermeiden, wurden alle Verbrauchsmaterialien mit Salpetersäure vorgereinigt. Letztendlich ermöglichte die Kombination von HPLC-ICP-MS/MS mit speziesspezifischer ID die genaue Quantifizierung von β-Amyloid-Standards mit hohem Durchsatz und geringem Probenverbrauch.

1. Introduction

1.1 Neurodegenerative diseases: An Overview

Progress in science and medicine lead to the eradication of many diseases in the 20th century, mostly infectious ones. These advances changed our life expectancy dramatically but left us with a new problem. We now have to deal with chronic diseases due to the aging process of our body, which are more complicate to deal with. In addition to their complexity, they are the consequence of years of development, which makes them very hard to predict. [1, 2]

If we compare studies from the World Health Organization (WHO) about the leading causes of deaths worldwide we can see a drastic increase on the side of chronic diseases (**Figure 1**). Especially cancer and different forms of dementia like Alzheimer's disease (AD) are rising every year, which is why in 2016 they are amongst the top 10 global causes of death. [3]

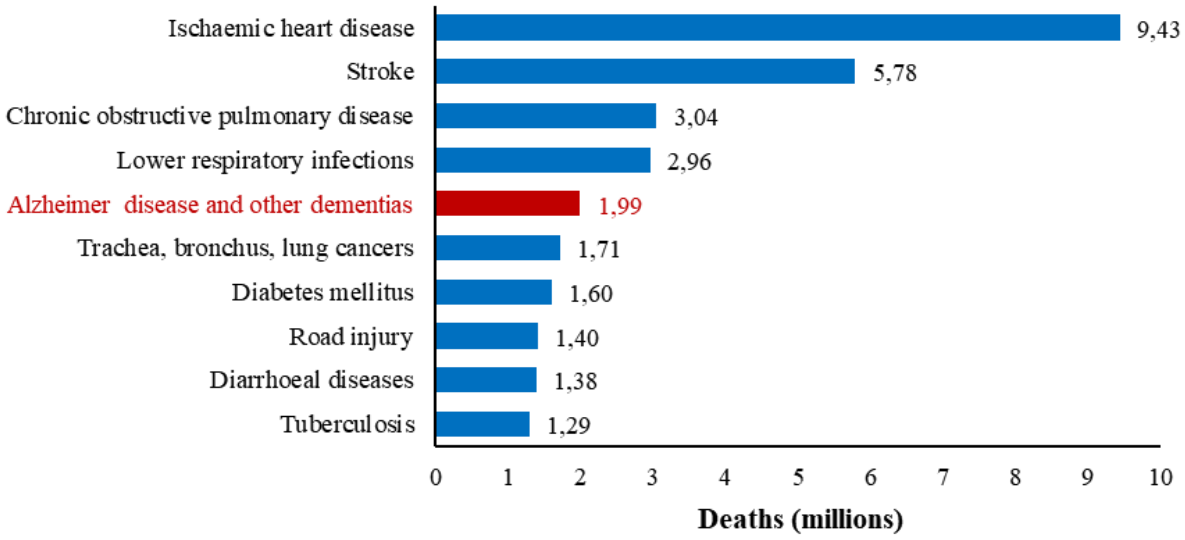

Figure 1: Top 10 global causes of deaths 2016 according to a report of the WHO [3]

A look at the statistics of countries with different income, makes this even clearer. While people with low-income are more likely to suffer from poor hygiene, bad nutrition and unclean environments and mostly die from viral or bacterial infections (e.g. lower respiratory infections, diarrheal diseases, HIV/AIDS) because of this, people with high income and good living conditions are more prone to die from age-related diseases (e.g. Ischaemic heart disease, dementia, cancer). [3]

Therefore, the investigation of Alzheimer and other neurodegenerative diseases is from utmost importance in the Western World. More than 6 million people in the European Union and 44.4 million people worldwide suffer from dementia with studies estimating that the numbers will double in the next 20 years. [4, 5]

Because of its complex nature there are currently no drugs available, which can deal with the disease itself, so the only option is symptomatic treatment. Acetylcholinesterase inhibitors like donepezil or galantamine for example are commonly used to reduce the memory loss of dementia patients by preventing the metabolic breakdown of acetylcholine, an important neurotransmitter. [5, 6]

So even if these neurodegenerative diseases are still fatal, treatment in its prodromal stages can significantly increase the life expectancy, as many studies suggest. That's why early diagnosis is very important. The problem here is the lack of reliable biomarkers, which can accurately determine the illness in these early stages. [4, 7]

In the case of the most abundant form of dementia, Alzheimer's disease, proteins and peptides related to the senile plaque like the β-amyloid peptide 1-42 or tau-protein are analysed in cerebrospinal fluid (CSF) via immunoassays or optical methods. Besides the fact, that these methods are often associated with inconsistent results, no real cut-off value was established for differentiating between healthy and sick people, thus resulting in wrong diagnoses, which can impact the life of a patient. [4, 8]

1.2 Alzheimer´s disease

The most common form of dementia, Alzheimer's disease, is estimated to account for nearly two-thirds of all disease cases, with the exact number fluctuating as the disorder is often not precisely identified or mistaken with other forms of dementia due to similar symptoms. A clear diagnosis is often made only after autopsy by pathological examination, with extracellular senile plaque (amyloid-β peptide) and neurofibrillary tangles (tau-protein) in the cortex or hippocampus of the brain considered to be characteristic for AD. [9]

As is common for dementia, there is a gradual loss of memory, language and other cognitive abilities. However, especially with AD, the neuronal damage in the brain spreads so much that motor functions of the body are also affected. This results in a continual deterioration in the quality

of life, where at some point basic body functions such as walking, swallowing or breathing are lost, ultimately ending in the death of the patient, mostly caused by their vulnerability to infections in this physical state (e.g. pneumonia). [9, 10]

Of course, the symptoms of the disease are different depending on the person. After initial memory loss, neurons in other brain regions begin to fail and eventually die. Depending on the affected region, there are different problems for the individual. Mood changes, depression, confusion, troubles with speaking and writing are just some examples for possible symptoms. [10]

As is often misunderstood, old age is not the cause of AD, it's just the biggest risk factor. It´s not a normal phenomenon of the aging process and can also occur in younger people, but of course to a much lesser extent, as you can see in **Figure 2**. For those under the age of 65, it is referred to as early-onset AD, making up 4% of those affected. This group of AD patients has a particularly high mortality rate because they are usually diagnosed too late, causing irreversible brain damage early. [10, 11]

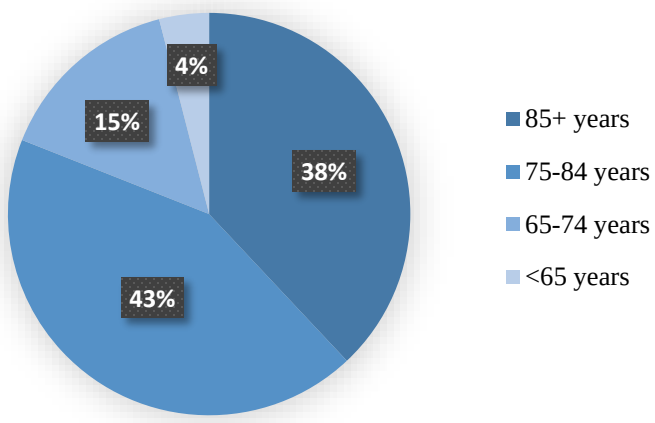

Figure 2: Ages of people with AD in the United States, 2015 [10]

In addition to age, other factors could be found that correlate with increased AD risk. Genetic mutations and the inheritance of certain genes (e.g. ε4 APOE gene) have had an impact on AD risk. People with first-degree relatives, such as parents or siblings that already had AD, should be mindful and pay attention to changes in their cognitive abilities. It has also been shown that having a healthy lifestyle can have a positive impact, as the health of the brain is related to the heart and blood cells. It is a modifiable parameter that we can influence in our lives through, for example, physical activity, eating healthy or not smoking. Higher education or mentally stimulating work

had also positive effects, but one should not judge prematurely here, as there are often other correlations, such as poorer health care or nutrition, resulting from the different degrees of education. [10]

1.3 β-Amyloid

Already since the early discovery of Alzheimer´s disease in 1907, the deposition of senile plaque and neurofibrillary tangles in the hippocampus of the brain has been recognized as a defining pathological feature, as big amounts could be found in dead patients. It therefore comes as no surprise that the focus of Alzheimer´s research has mostly been on this topic. [12-14]

Specifically, the major component of this deposit is being researched, a peptide called amyloid-β (Aβ), which consists of 38-42 amino acids. In the body it is formed by sequentially cleaving the C-99 fragment from the transmembrane protein APP (amyloid β precursor protein) using the β-site APP cleaving enzyme (BACE1). γ-Secretase then allows the formation of different Aβ-peptide species from this fragment. If the α-secretase (ADAM-10) dominates over the β one, the neuroprotective peptide sAPPα is built instead of Aβ. The different pathways are illustrated in **Figure 3**. [12, 13, 15, 16]

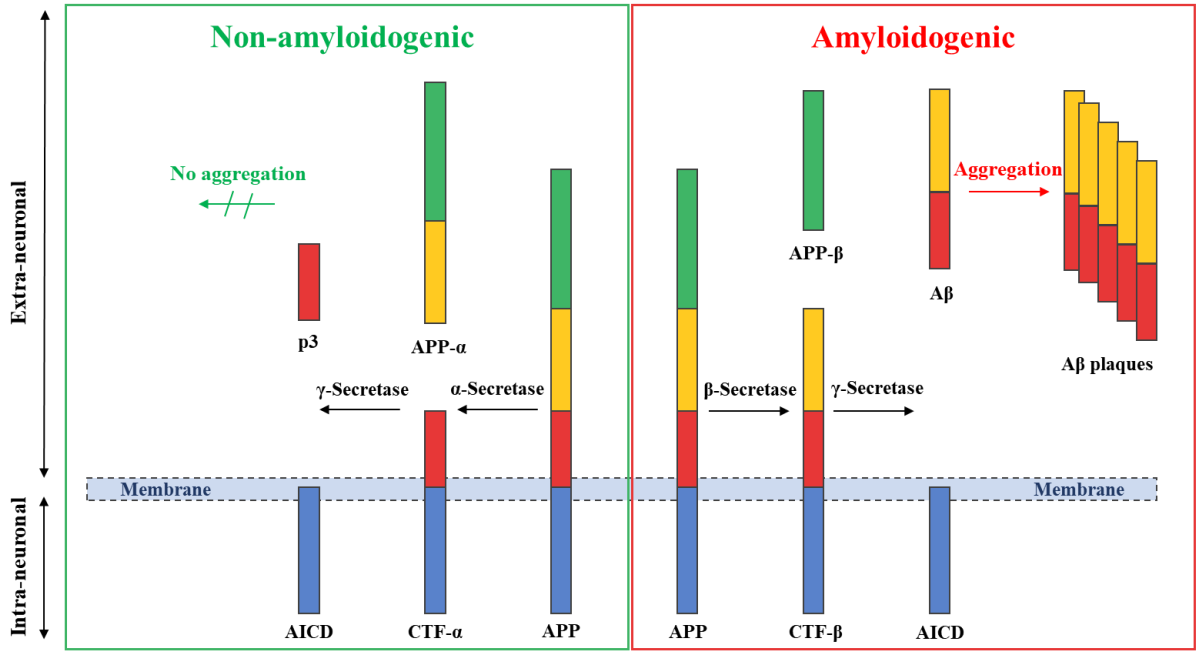

Figure 3: The different pathways of APP [17]

This process mainly takes place in the neurons and astrocytes of the brain, however, Aβ can also be formed in other regions such as the skin or skeletal muscle. After storage in the extracellular space, Aβ is transferred in soluble form into the cerebrospinal fluid (CSF) and can be transported from there, whereby mainly the $A\beta_{40}$ (2-3 µg L^{-1}) and $A\beta_{42}$ (0,7-0,8 µg L^{-1}) species occur in healthy individuals. [13]

Binding to other amyloid beta peptides may result in the formation of complex oligomers that are significantly more difficult to remove from the brain and thus form poorly soluble plaque over time, which has been shown to be neurotoxic in many studies. The mechanism of this oligomerization is relatively well understood. It´s an attempt of numerous Aβ molecules to minimize their final free energy by building bigger aggregates using the lipid membrane. So, the utilization of the membrane plays an important role as experiments showed less activity of Aβ in pure solutions. The formation of the oligomers takes place stepwise with conformational transitions, which differ in their solubility, toxicity and peptide length. Since clinical trials have found that plaque removal neither reverses neuronal damage nor stops AD, more recent studies indicate that oligomers could be the primary source for toxic effects, instead of the insoluble fibrils. [13, 18, 19]

Although it is currently not possible to say which species of amyloid beta specifically causes toxicity, some of the effects that cause neuronal damage are already known. Above all, the emergence of reactive oxygen species (ROS) and the associated oxidative stress play an important role. Due to structural similarities of the Aβ peptide with other metal ligands such as metallothionein (binding of Cu to 2 histidine groups), metals like Cu or Zn can be bound with relatively high affinity. As a result, especially Cu may be present as a reactive redox component, resulting in a catalytic cycle between Cu (I) and Cu (II), which in the presence of a reducing agent (e.g. ascorbate) creates ROS such as $O_2^{\cdot -}$, H_2O_2 or $OH^{\cdot}$ out of oxygen. These in turn can cause oxidative damage to different parts of the brain. [20-22]

Based on this knowledge, many researchers have focused on fighting AD by removing Aβ or inhibiting its creation. However, the treatments were not successful, as monomeric Aβ itself is an important peptide in our body, that shows functions within the physiology of a healthy human. In addition to its role in synaptic regulation and protection of neurons, other beneficial properties have been found like tumor suppression or antioxidative activity. [13, 23, 24]

So, according to the current state of knowledge, it is most important to find out which mechanisms are responsible for increasing the conversion of Aβ into toxic oligomers and preventing them instead of inhibiting the production of Aβ and its precursor protein APP.

1.4 Biomarkers for Alzheimer

Depending on the condition and age of a patient, Alzheimer´s disease can cause very different symptoms, making accurate diagnosis difficult. While early-onset AD patients are easily identified by severe neuropathological changes (senile plaque, neurofibrillary tangles), later cases are often indistinguishable from unaffected elderly due to their pathophysiological heterogeneity. [25, 26]

Therefore, there was a demand for suitable biomarkers, especially those in biological fluids, as these are more readily available and have a major impact on most medical decisions. For AD and other neurodegenerative diseases, cerebrospinal fluid was chosen, as it is in direct contact with the brain parenchyma, unlike blood, and thus contains secreted proteins from the brain. However, to extract CSF, a lumbar puncture is needed, in which a needle is inserted into the spinal canal, making repeated sampling over a long period of time difficult. In 1992 Aβ was proven to be secreted into CSF, which triggered the development of many different immunoassays. Finally, in 1995, an ELISA method was developed which showed a lower Aβ42 content for AD patients compared to the control group. This finding was confirmed in numerous subsequent papers. An explanation for this was found in the following years. It was shown that free Aβ42 is lost by aggregation to oligomers and eventually plaques, which leads to less amyloid secretion into the CSF. [25, 27, 28]

This fibril Aβ could also be visualized via positron emission tomography (**Figure 4**), thus, providing a new diagnostic method for AD, which showed similar results to CSF measurements. Here, the patient is injected with a weak radioactive substance such as ^{18}F-fluorodeoxyglucose (analog of glucose), which attaches with high specificity and sensitivity to the Aβ deposits. However, since PET provides different information (regional distribution) about the disease, it can be helpful to combine both methods to minimize the uncertainty of the diagnosis. [25, 29-31]

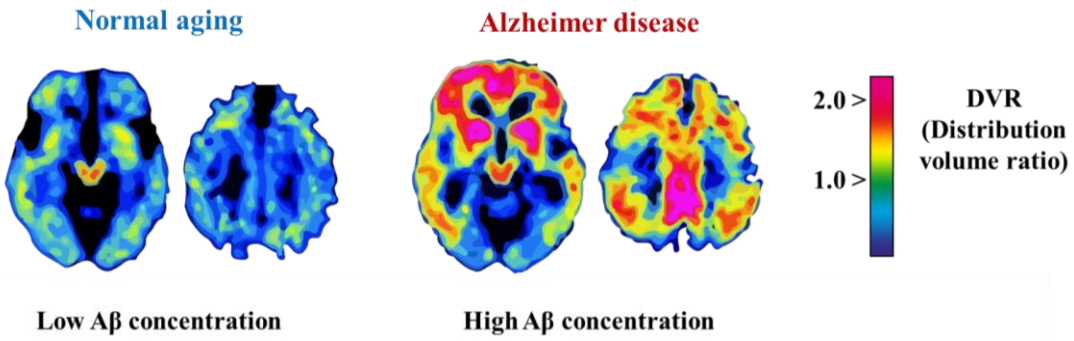

Figure 4: PET scan with Aβ plaque bound to Pittsburgh Compound B [32]

In addition to Aβ42, numerous other fragments were later found in human CSF, with Aβ40 being the most abundant one (10 times higher concentration than Aβ42). Although Aβ40 itself shows no or only minor changes in AD patients, measuring the Aβ42/Aβ40 ratio significantly improved the accuracy of the results compared to using only Aβ42 as biomarker (normalization of differences in CSF). Since neurofibrillary tangles play a major role in the pathology of AD besides Aβ plaques, there was of course also a focus on the tau proteins contained therein. To begin with, the total tau content (T-tau) was analysed by means of ELISA in CSF, as the distinction of all six tau isoforms was too difficult. Patients who have suffered neuronal damage showed an increased T-tau concentration in CSF. Although it was possible to identify AD patients, the method was too unspecific to differentiate AD from other neurodegenerative diseases such as Creutzfeldt-Jakob disease or acute brain damage. So, the method was more of an indicator for the severity of neuronal damage. [25, 33]

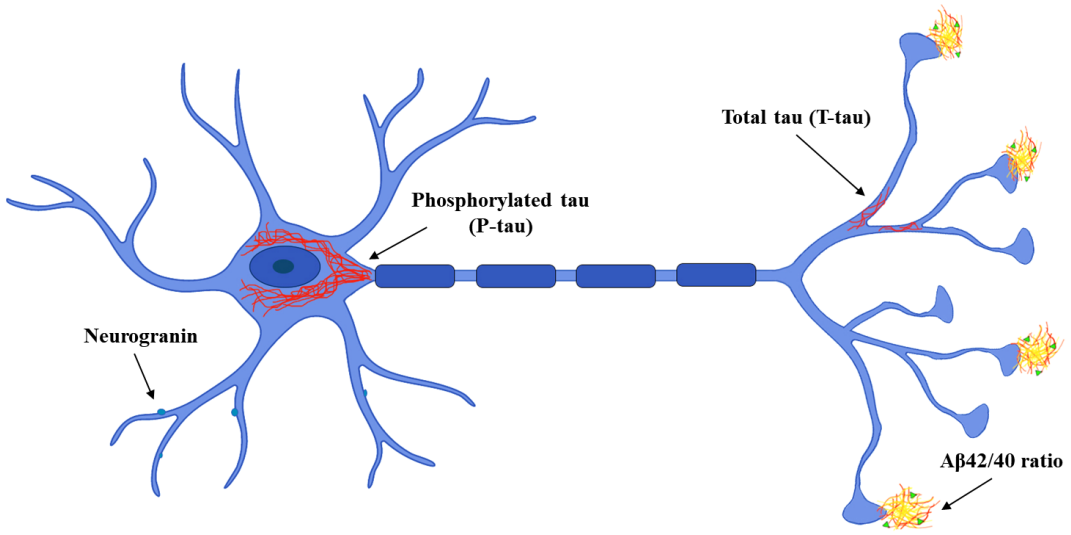

Figure 5: Overview of the AD biomarkers in a damaged neuron [25]

However, by specifically targeting phosphorylated tau proteins with known post-translational modifications, differentiation of AD from other disorders is made possible. Particularly an increase of P-Tau181, P-Tau199 and P-Tau231 showed great correlation with AD. [25, 34]

To date, the biomarkers mentioned are used. In recent years, the focus has been on standardization (e.g. certified reference materials of Aβ42 in CSF, reference measurements with mass spectrometry) and automation of the methods. A major problem, however, is that the onset of AD still cannot be diagnosed, and thus the symptomatic treatment occurs too late, causing irreversible damage. Low Aβ42 in CSF is the only biomarker that showed the ability to predict cognitive decline in advance but just 8 years before, which is often too late. Above all, it must be taken into account that the removal of CSF is an invasive method, which is usually not used preventively. Blood would be the better alternative, however, only low concentrations of established biomarkers are present, which is why new research is carried out to search for alternatives like metals or metalloproteins (e.g. ferritin). [4, 25, 35]

1.5 ICP-MS

Inductively coupled plasma-mass spectrometry (ICP-MS), being a hard ionization technique, has proven to be an outstanding method for elemental analysis in biological and environmental samples, as it allows the quantification of numerous elements even in complex matrix with only a small amount of sample preparation. In addition to its multielement capabilities, low detection limits and high dynamic range, it also has many opportunities for on-line coupling with separation techniques, such as HPLC, GC or CE, making it ideal for speciation analysis. [36, 37]

The measurement of isotopic compositions also allows the use of advanced standardization methods such as isotope dilution analysis, making measurements even more reliable. [38]

In the case of aqueous solutions, samples are pumped directly into the nebulizer (e.g. through HPLC, peristaltic pump), while orthogonally an argon gas flow is introduced, which generates pneumatic force, thereby forming a fine aerosol, which is forwarded into the spray chamber. Here, depending on the spray chamber used, the large droplets are separated by either centrifugal (cyclonic) or gravitational (Scott type) forces to avoid poor dissociation or strong oxide formation in the plasma. Only a small fraction of the original sample solution (<1%) gets into the plasma,

where the high temperatures (6000-10000 K) gradually leads to vaporization, atomization and finally ionization, which is why only elemental information can be obtained. [39]

Figure 6: Close-up of inductively coupled plasma in an ICP-MS instrument

The interface region, consisting of sampler and skimmer cone, is responsible for the coupling of ICP to MS, as a transition from atmospheric pressure to high vacuum is required. In order to reduce the background noise, an ion optic composed of several electrostatic lenses is used, which is capable of removing neutral species, negatively charged ions and photons (interfering matrix), resulting in enhanced efficiency. By applying a positive voltage, ions drifting outward are also refocused and transferred to the mass analyser, where they are separated according to their mass-to-charge-ratio (m/z).

Depending on the requirements regarding resolution, accuracy and data acquisition speed there are different mass analysers available, each with their respective field of application. In the early days of ICP-MS mainly simple quadrupole mass filters were used. However, since these were not suitable for the analysis of difficult elements such as As, Fe or Se or complex matrices (e.g. serum, CSF) because of their low resolution, other techniques were developed. In the following, function and use of the three main techniques will be described. [40-42]

Table 1: Quadrupole mass filter

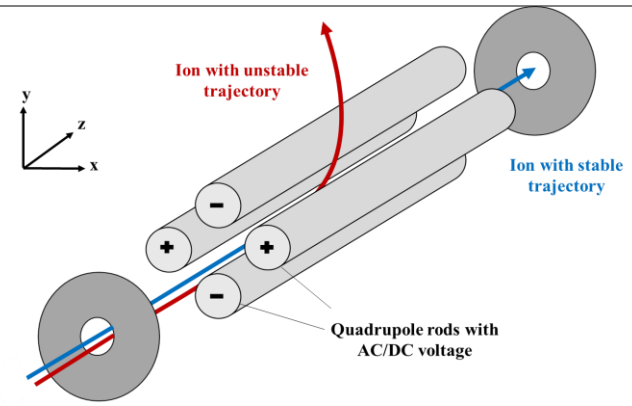

[43]

Short description	Within a quadrupole system, ions enter a square array of 4 electrode rods (z-direction), where each pair of rods is controlled by DC (U) and RF (V) potentials, creating oscillation (x-y plane). Depending on the applied U and V values, only specific ions are able to reach the detector (stable trajectory), resulting in separation based on their mass-to-charge ratio. [43-45]
Advantages	Low price, easy handling, fast scan speed, high sensitivity [41, 42, 46]
Disadvantages	Low mass resolution (~300), poor precision (isotope ratios) [46, 47]

Table 2: Double-focusing sector field mass spectrometry

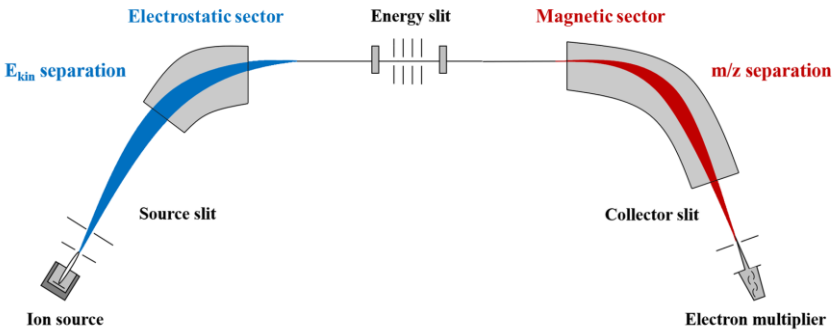

[48]

Short description	Double-focusing sector field devices are composed of an electrostatic (ESA) and magnetic sector. The ESA results in energy dispersion, which narrows the distribution of kinetic energy, allowing the ion beam to be focused. Subsequently, the ions arriving orthogonally into the magnetic field are separated on the basis of their momentum (Lorentz force) and thus their m/z ratio. The geometry and order of the sectors can vary, depending on the design of the instrument. [45]
Advantages	High mass resolution (~8000-10000), high precision (isotope ratios) [42, 46]
Disadvantages	High price, time consuming [46]

Table 3: Time of flight mass spectrometry

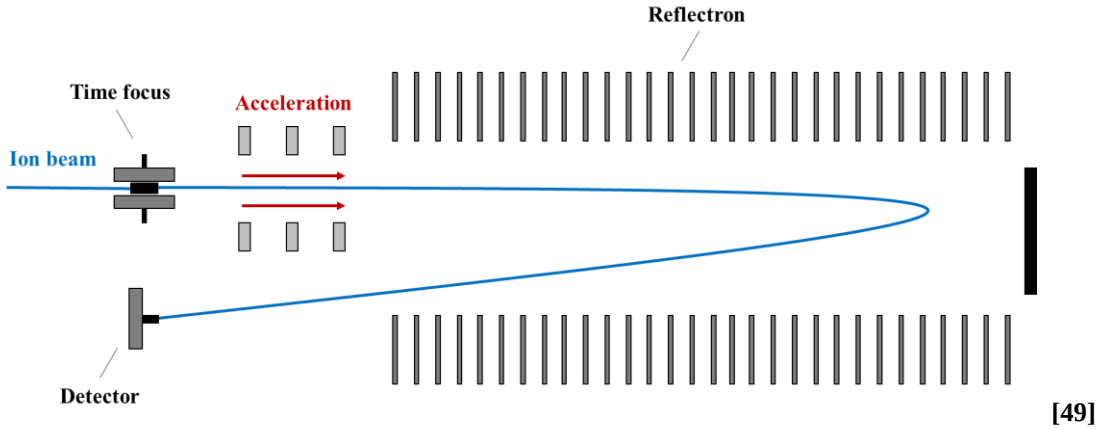

[49]

Short description	In time-of-flight mass spectrometry ions are accelerated within a homogenous electric field and drift through a field-free region. Since the ions experience the same kinetic energy, the masses are separated according to their different times of flight. However, energetic deviations can occur, which is why reflectrons are commonly used, that are able to focus different energies of the ion beam in time. [45, 49]
Advantages	High mass resolution (~8000-10000), simultaneous measurements [42, 49]
Disadvantages	Lower sensitivity and dynamic range [45]

After separation of the ions in the mass analyser, they finally arrive at the detector, typically a secondary electron multiplier (SEM), which generates signals that are integrated via the software of the instrument. However, the detector can also be extended with Faraday cups (MC-ICP-MS) in addition to the SEM, which enables a more precise measurement of isotope ratios. [39, 50, 51]

1.5.1 Interferences

Due to the low resolution (approximately unit mass) of quadrupole-based ICP-MS, which accounts for up to 90% of commercially available devices, their analytical performance is largely affected by spectral interferences. These interferences are ions with the same m/z ratio, which leads to an increased background of the analyte and thus falsifies the results (false positive). A distinction is made between isobaric interferences, polyatomic ions and doubly charged ions. **Table 4** shows examples for the respective type of interference. [39, 52, 53]

Table 4: Different types of spectral interferences

Type of interference	Example
Isobaric interference	$^{87}Rb^{+}$ => $^{87}Sr^{+}$
Polyatomic ions	$^{40}Ar^{16}O^{+}$ => $^{56}Fe^{+}$
Doubly charged ions	$^{140}Ce^{2+}$ => $^{70}Zn^{+}$

In particular, the formation of polyatoms plays a major role, because unlike isobaric interferences, which are more specific to the sample itself, they are formed from plasma, atmospheric gases, and the matrix. To prevent this, newer ICP-MS devices are additionally equipped with a dynamic reaction cell (hexa- or octupole), which enables the removal of interferences though controlled collisions and reactions inside of the cell, resulting in increased selectivity but decreased sensitivity. [54]

Within the collision mode, ions collide with an inert gas such as He, which causes a reduction of their kinetic energy. Since polyatomic species have a significantly larger cross-section than atomic ions of the same mass, they are more prone to collide, resulting in a bigger energy loss. In the end, the interferences can be separated using kinetic energy discrimination. [55]

When using reactive gases such as H_2, O_2 or NH_3, there are targeted reactions either with the interfering matrix (e.g. removal of $^{40}Ar^{+}$ with H_2), which allows the measurement at the original m/z ratio, or with the analyte ions, which shifts their m/z into a more measurable range. Below are some of the reactions that can reduce interferences.

Table 5: Typical reactions leading to a reduction of interference [56, 57]

Reaction	Chemical equation
Charge transfer	$^{40}Ar^{+} + {}^{1}H_2 \rightarrow {}^{1}H_2^{+} + {}^{40}Ar$
Proton transfer	$^{40}Ar^{1}H^{+} + {}^{1}H_2 \rightarrow {}^{1}H_3^{+} + {}^{40}Ar$
Hydrogen transfer	$^{40}Ar^{+} + {}^{1}H_2 \rightarrow {}^{40}Ar^{1}H^{+} + {}^{1}H$
Oxidation	$^{32}S^{+} + {}^{16}O_2 \rightarrow {}^{32}S^{16}O^{+} + {}^{16}O$

While H_2 and O_2 are relatively easy to use due to their small number of reaction products, NH_3 looks much more complex, but offers greater flexibility in return. This enables, for example, the

measurement of titanium in biological samples using $^{48}Ti(NH_3)_6$, which would otherwise not be possible in any other mode due to the high ^{48}Ca interference. [58]

1.5.2 Tandem mass spectrometry (ICP-MS/MS)

ICP-MS/MS represents an extension of quadrupole-based technology. In addition to the normal setup, another quadrupole is connected in front of the dynamic reaction cell, as you can see in **Figure 7**, which is why it is also referred to as triple quadrupole (ICP-QQQ) instrument. The analysis is thus expanded by a further separation step, since only ions with a specific m/z ratio get into the CRC, thereby avoiding unwanted reaction products. This enables a high degree of selectivity, that is able to compete with the mass resolution of sector-field instruments but requires significantly less measurement time and lower acquisition cost. [59-61]

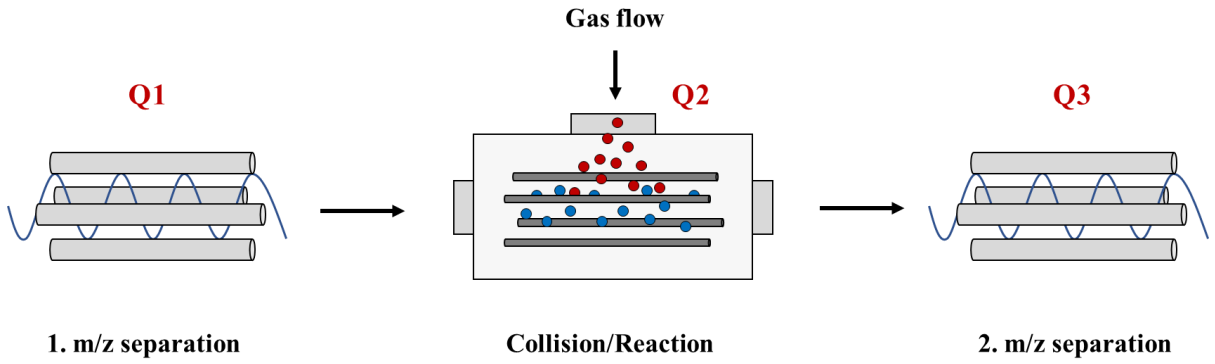

Figure 7: Triple quadrupole setup of an ICP-MS/MS

There are two approaches to avoid spectral overlap: on-mass and mass-shift. In both cases the m/z of the most abundant or interference-free isotope is selected for the first quadrupole (Q1) and these ions react in the CRC. Depending on the measured element and sample matrix, the original m/z is used for Q2 (on-mass) or that of an abundant reaction product (mass-shift). The reaction behavior of the analyte in the CRC is therefore crucial for this decision. In general, however, the mass-shift approach has a wider range of application since removing matrix in a targeted manner often proves to be more difficult than just shifting the m/z of the analyte. A typical example for this is the measurement of sulfur in oxygen mode (**Figure 8**), which has been significantly improved by the triple quadrupole technology, since the selection in Q1 at m/z = 32 avoids unnecessary reaction products, thus making the measurement of $^{32}S^{16}O^+$ at m/z = 48 in Q2 relatively interference-free. [59, 62]

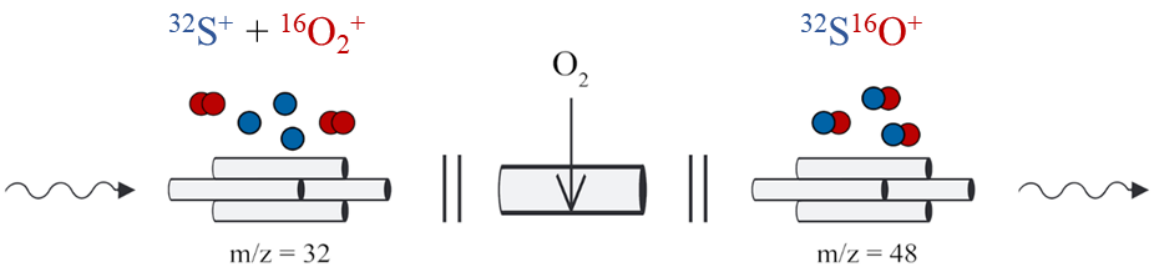

Figure 8: Sulfur measurement in oxygen mode with mass-shift approach (Q1: m/z = 32, Q2: m/z = 48)

Nevertheless, the on-mass approach also has its use, for example when measuring ^{56}Fe with NH_3, where the abundant $^{40}Ar^{16}O^+$ ion can be removed via a charge transfer reaction, which allows the analysis at m/z = 56 in Q2. [59]

However, measurements should only be done in MS/MS mode if it is necessary for the element (SQ possible) because any kind of further selection leads to a reduction in ion transmission efficiency and consequently sensitivity. In summary, it can be said that ICP-MS/MS made it possible to monitor and control the processes (reaction products, interferences) within the CRC, thus enhancing the capability of the instrument to overcome spectral interferences. [59-61]

1.6 Speciation analysis

Speciation analysis is a research area that deals with the characterization and quantification of chemical species. According to IUPAC, a species is defined as: "Specific form of an element defined as to isotopic composition, electronic or oxidation state, and/or complex or molecular structure." [63]

Thus, it is a relatively broad term, but in the narrower context of mass spectrometry mostly relates to the molecular form of an element. Knowing the nature of the species is of great importance as it provides further physicochemical information like toxicity, biological functions or mobility. A frequently observed element in the environment, for example, is mercury, since its forms (organomercury compounds, Hg^{2+}, Hg^0) vary greatly in their toxicity, making distinctions necessary. [64, 65]

ICP-MS in combination with HPLC has proven particularly useful for this research area. The chromatographic separation provides specific molecular information, while the ICP-MS serves as a robust detector that only depends on the element concentration, making quantification much

easier compared to ESI-MS, which has different ionization efficiencies for each molecule. However, it must also be taken into account that ICP-MS is limited in the selection of organic solvents, since these have a significant influence on the stability of the plasma and thus affect the performance of the instrument (sensitivity). [64, 66-68]

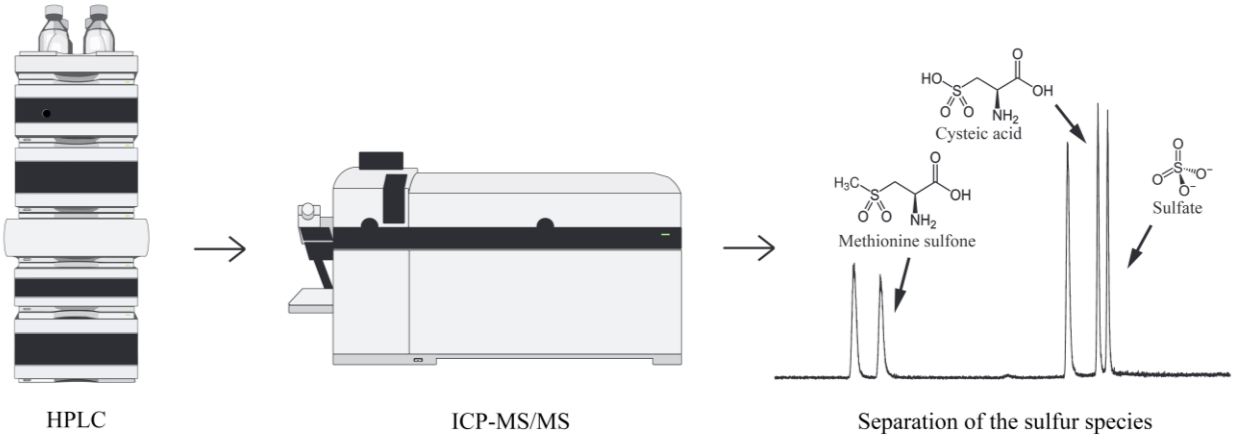

Figure 9: Separation of sulfur-species through HPLC-ICP-MS/MS

Generally, there are two different approaches in speciation analysis: targeted and non-targeted. The area of targeted analysis mainly deals with method development for already known species. It is therefore a matter of obtaining accurate and precise data through advanced methods such as species-specific isotope dilution, which is why it has become particularly important for the monitoring of toxic substances in our environment. In comparison, with non-targeted analysis you have to do more fundamental research because the analyte is unknown. Here, in order to determine novel species, it can be helpful to use molecular (ESI-MS) in addition to elemental (ICP-MS) mass spectrometry. [64]

While these methods were initially used primarily for environmental or food related issues (As, Hg, Cr), technical advances (e.g. ICP-MS/MS) made it possible to also answer pharmaceutical or medical problems by analysing non-metals like sulfur, phosphorus or selenium, which previously suffered from low sensitivity or excessive interferences. Since these elements are an important component of biologically functional molecules such as proteins, lipids or other metabolites, their analysis can provide an insight into biological processes. [66, 69, 70]

1.7 Isotope dilution mass spectrometry

The basic principle of isotope dilution is the modification of the isotope ratios of an element through the addition of an isotopically enriched or labeled form of the same element with known composition. This means that the added standard differs only in mass but is otherwise identical in its properties, making it ideal for comparison, since the matrix has the same effect on it. Because the sample and internal standard are simultaneously measured as a mixture, no further calibration is necessary. [71]

For example, when measuring sulfur, the sample has a natural isotope composition, consisting of about 95% ^{32}S and 4% ^{34}S. By adding a spike enriched in ^{34}S (>99%), a mixture with new isotope ratio is created. Ideally, the concentrations are adjusted so that the two target isotopes are at a similar level. The original concentration of the sample can now be determined using the new isotope ratio, since the composition of the spike is known.

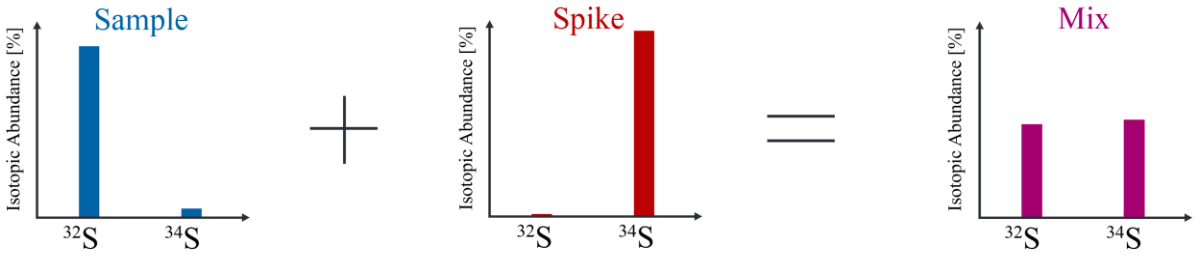

Figure 10: Schematic representation of the isotope dilution analysis using $^{32}S/^{34}S$

The calculation is carried out using the following equation:

Equation 1: Calculation of the sample concentration using isotope dilution

$$C_x = \frac{C_s \cdot m_s}{m_x} \cdot \frac{R_s - R_b}{R_b - R_x} \cdot \frac{f_{Bs}}{f_{Bx}}$$

c_s	Concentration of spike
c_x	Concentration of sample
m_s	Mass of spike
m_x	Mass of sample
f_{As}	Abundance of isotope A in spike

f_{Bs}	Abundance of isotope B in spike
f_{Ax}	Abundance of isotope A in sample
f_{Bx}	Abundance of isotope B in sample
R_b	Ratio of $^{32}S/^{34}S$ in blend
R_s	f_{As}/f_{Bs}
R_x	f_{Ax}/f_{Bx}

Since isotope dilution enables accurate results even in complex matrixes, it is not surprising that this technique has established itself as a useful tool in speciation analysis. Depending on the application, one of two different approaches is used for spiking, either species-specific or species-unspecific isotope dilution.

1.7.1 Species-specific isotope dilution

For this type of analysis, isotopically labeled forms of the examined species are added during sample preparation, which means that losses before the measurement are compensated. It is therefore similar to classic labeling in organic mass spectrometry, where ^{2}H and ^{13}C are used in internal standards for accurate quantification. However, since ICP-MS is used as a detector, the isotopic composition of the heteroatoms is usually changed instead (e.g.$^{32}S/^{34}S$ in methionine or $^{77}Se/^{78}Se$ in selenocysteine), making this procedure even more specific. [72-76]

It must be taken into account that this type of isotope dilution is limited by the availability of labeled standards. Even if there are some commercially available, they are still very expensive, which is why you often have to rely on independent synthesis. There are mainly two approaches to this found in literature. Either specific cell cultures are used that are grown with labeled substrates and thus produce the required molecule, or they are formed by direct synthesis or modification via numerous reactions. With both methods, however, there is the problem that the production is complex and only low efficiency is achieved, which also explains the high price of commercial standards. That is why method development has become very important in this area. [71, 75]

The ^{34}S-labeled amino acids used for this work were produced, for example, by fermentation from yeast with ^{34}S-labeled sodium sulfate as the substrate, as can be seen in **Figure 11**. The method for this was published by Gerrit Hermann et al. in 2016 and is also used for labeling metabolites with ^{13}C. [73, 77, 78]

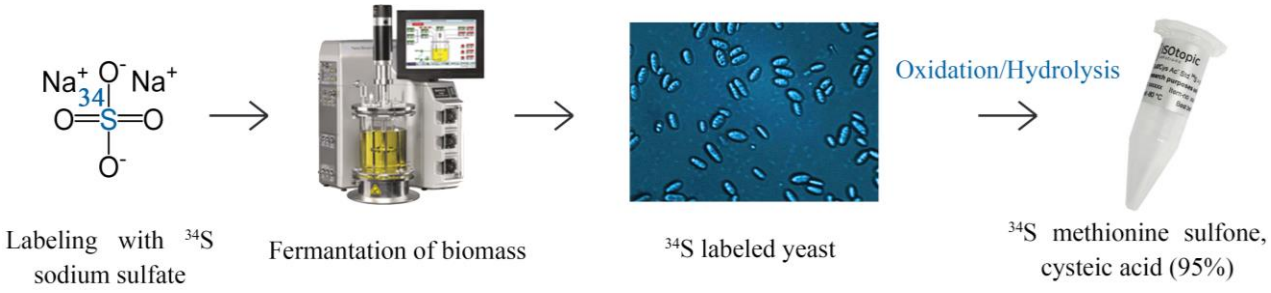

Figure 11: Synthesis of ^{34}S-labeled amino acids by fermentation with yeast [77, 79]

1.7.2 Species-unspecific isotope dilution

As the name suggests, the standard is not selectively adapted to the analyte, which makes this method versatile on the one hand, but also unspecific, correcting only for instrumental errors. The on-line approach has prevailed here, using a post-column spike that is enriched in another isotope. By continuously adding the spike during the measurement, sample preparation is significantly reduced and precipitation within the sample solution can be avoided. [72, 80]

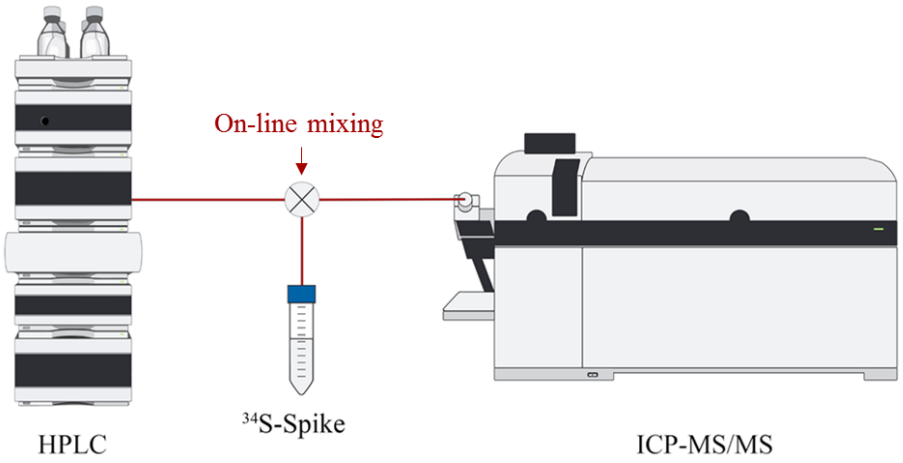

Figure 12: Setup for the measurement of sulfur using online isotope dilution

A modified version of the isotope dilution equation is used here, since a time-dependent mass flow is measured, from which the concentration is then finally determined via integration.

Equation 2: Calculation of the mass flow using on-line isotope dilution

$$M_x(t) = M_y(t) \frac{R_y - R_b(t)}{R_b(t) - R_x} \cdot \frac{f_{Bs}}{f_{As}}$$

$M_x(t)$	Mass flow of sample
$M_y(t)$	Mass flow of spike
f_{As}	Isotopic abundance of ^{32}S in spike
f_{Bs}	Isotopic abundance of ^{34}S in spike
$R_b(t)$	Ratio of $^{32}S/^{34}S$ in blend (time-dependent)
R_x	Ratio of $^{32}S/^{34}S$ in sample
R_y	Ratio of $^{32}S/^{34}S$ in spike

Due to the addition of the spike via a peristaltic pump, it is important to maintain a constant flow rate, otherwise there can be a lot of noise caused by fluctuations (**Figure 13**), which lead to errors in the integration, ultimately affecting the final results. It is therefore recommended to monitor the mass flow gravimetrically by using a balance, especially when working with small concentrations. [81]

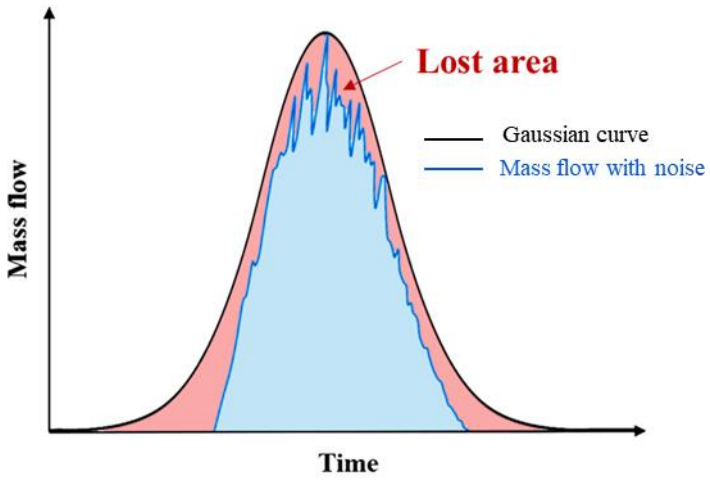

Figure 13: Comparison of a mass flow chromatogram containing noise with an ideal gaussian curve [81]

2. Experimental Part

2.1 Reagents and materials

The amino acid standards, namely cystine, cysteine, cysteic acid, methionine and methionine sulfone, were purchased by Sigma Aldrich (Steinheim, Germany). Both purity grades of lysozyme (from chicken white egg) and myoglobin (from equine skeletal muscle) were also purchased by Sigma Aldrich. The synthetic β-Amyloid standards (Aβ40, Aβ42) were purchased by r-Peptide (Georgia, USA). ^{34}S-labeled yeast hydrolysates containing methionine sulfone and cysteic acid were kindly provided by ISOtopic solutions (Vienna, Austria), while ^{34}S sodium sulfate (abundance ~ 99.9%) was bought by Eurisotop (St-Aubin, France). All acids and bases with Suprapur purity were purchased by Lactan (Graz, Austria). Ultrapure water (18.2 MΩ cm, Milli-Q Advantage, Darmstadt, Germany) was used for all dilutions and buffer preparation.

The following table lists the details of the chemicals:

Table 6: List of chemicals

Reagent	Purity	Storage conditions	Molar mass [g mol^{-1}]	CAS	Hazards	Precautions
HCl	35%, Suprapur	sufficient ventilation	36.46	7647-01-0	H290-H314-H335	P261-P280-P301 + P330 + P331-P303 + P361 + P353-P304 + P340 + P310-P305 + P351 + P338 + P310
HNO_3	69%, Suprapur	sufficient ventilation	63.01	7697-37-2	H272-H290-H314	P210-P220-P260-P280-P305 + P351 + P338-P370 + P378
NH_3	25%, Suprapur	sufficient ventilation, cooling	35.05	1336-21-6	H290-H314-H335-H400	P273-P280-P301 + 330 + 331-P305 + P351 + P338-P308 + P310

HAc	100%, Suprapur	sufficient ventilation	60.05	64-19-7	H226-H314	P210-P260-P280-P303 + P361 + P353-P305 + P351 + P338-P370 + P378
H_2O_2	30%, Suprapur	sufficient ventilation	34.01	7722-84-1	H302-H318-H413	P273-P280-P305 + P351 + P338-P313
Formic acid	98-100%, Suprapur	sufficient ventilation	46.03	64-18-6	H226-H302-H314-H331	P210-P280-P301 + P330 + P331-P304 + P340-P305 + P351 + P338-P308 + P310
MeOH	≥99.9%, for HPLC	r.t.	32.04	67-56-1	H225-H301 + H311 + H331-H370	P210-P280-P301 + P310 + P330-P302 + P352 + P312-P304 + P340 + P311
Phenol	≥99%, purified by redestillation	sufficient ventilation, poison storage	94.11	108-95-2	H301 + H311 + H331-H314-H341-H373	P280-P301 + P330 + P331-P302 + P352-P304 + P340-P305 + P351 + P338-P308 + P310
Ar	5.0 (99.9990%)	pressurized gas	39.95	7440-37-1	H280	P403
L-Cystine	≥99.7%, TLC	r.t.	240,30	56-89-3	-	-
L-Cysteine	97%	r.t.	121,16	52-90-4	-	-
L-Methionine	≥98.0%, reagent grade (HPLC)	r.t.	149,21	63-68-3	-	-
L-Cysteic acid monohydrate	≥99.0%	r.t.	187.17	23537-25-9	-	-
DL-Methionine sulfone	≥99.0%	r.t.	181.21	820-10-0	-	-

Aβ40	>97.0%	-20°C	4331.50	-	-	-
Aβ42	>98.0%	-20°C	4514.10	-	-	-
Lysozyme	≥99.0%, VETRANAL™	2-8°C	14313,14	12650-88-3	-	-
Lysozyme	≥90.0%	2-8°C	14313,14	12650-88-3	-	-
Myoglobin	≥98.0%, SDS-PAGE	-20°C	17015,48	100684-32-0	-	-
Myoglobin	95-100%	-20°C	17015,48	100684-32-0	-	-
^{34}S-labeled yeast hydrolysate	>95.0%	-80°C	-	-	-	-
^{34}S sodium sulfate	>98.0%	r.t.	33.97	7704-34-9	H315	-

2.2 Instrumentation

For determination of the sulfur content, an Agilent 8800 ICP-MS/MS (Agilent Technologies, Tokyo, Japan) with oxygen as reaction gas ($^{32}S^{16}O$) was being employed. The instrument was coupled to an Agilent 1260 Infinity Bio-Inert HPLC system (Agilent Technologies, Waldbronn, Germany). The Agilent MassHunter software package (Workstation Software, Version C.01.03, 2016) was used for data evaluation. The instrumental parameters for the ICP-MS are summarized in **Table 7.**

Table 7: Instrumental parameters for the ICP-MS measurements

RF power	1550 W
Sampling depth	6.3 mm
Nebulizer	MicroMist
Spray chamber	Scott double-pass
Spraying chamber temp.	2°C
Monitored Isotopes	^{32}S, ^{33}S, ^{34}S, ^{36}S
m/z measured	48, 49, 50, 52
Plasma gas	15 L min^{-1}

Nebulizer gas	1.11 L min^{-1}
Auxiliary gas	0.90 L min^{-1}
Reaction gas	0,32 ml min^{-1} O_2
Cones	Ni
Cell entrance	-60 V
Cell exit	-110 V
Mode	TRA
Integration time	0.1 s
Measurement time	960 s
Repetitions	1

The final separation of the sulfur containing amino acids was carried out with a Thermo Scientific Dionex™ IonPac™ AS22 anion exchange column (Thermo Scientific Inc., Massachusetts, USA). In preliminary experiments other columns with reversed phase chemistry, specifically Atlantis T3 (3 µm, 4.6 x 150 mm, Waters) were tried out, but with insufficient results, which is why only the HPLC parameters of the anion exchange column are shown below in **Table 9.** The separation of the whole proteins and peptides for the determination of purity was finally carried out with an Acquity UPLC Protein BEH SEC Column (1.7 µm, 4.6 x 150 mm, 1-80K, Waters). The HPLC parameters were identical. The only difference is that 50 mM NH_4Ac was used as isocratic eluent.

Table 8: Column specifications

	Atlantis T3	**Dionex IonPac AS22**	**Acquity UPLC SEC**
Column type	Reversed phase	Anion exchange	Size exclusion
Material	Silica	PEEK	BEH
Particle size [µm]	3	6	1.7
Pore size [Å]	100	-	150
Length [mm]	150	250	150
Inner diameter [mm]	4.6	4.6	4.6

Table 9: HPLC parameters

Autosampler temp.	4°C
Injection volume	10 µL
Flow rate	400 µL min^{-1}
Column	Thermo Scientific Dionex™ IonPac™ AS22
Particle size	6 µm
Column specifications	2 x 250 mm
Column type	Strong anion exchange (Carbonate/Bicarbonate)
Column temp.	30°C
Eluents	A: 20 mM NH4Ac, pH = 8.0
	B: 400 mM NH4Ac, pH = 8.0
Gradient	0 – 4 min, 100% A
	4 – 7 min, Ramp to 100% B
	7 – 12 min, 100% B
	12 – 12.1 min, Ramp to 100% A
	12.1 – 16 min, 100% A

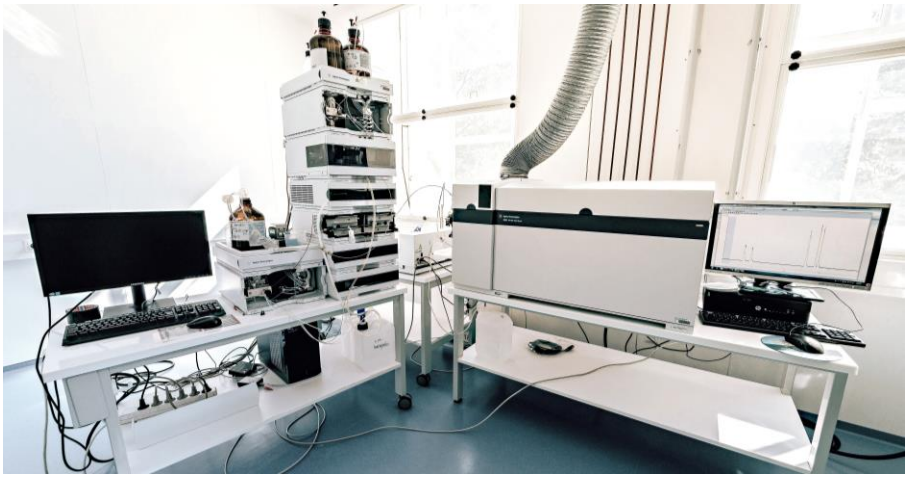

Figure 14: Agilent 1260 Bio-Inert LC coupled with Agilent 8800 ICP-MS/MS in a clean room environment (ISO class 7)

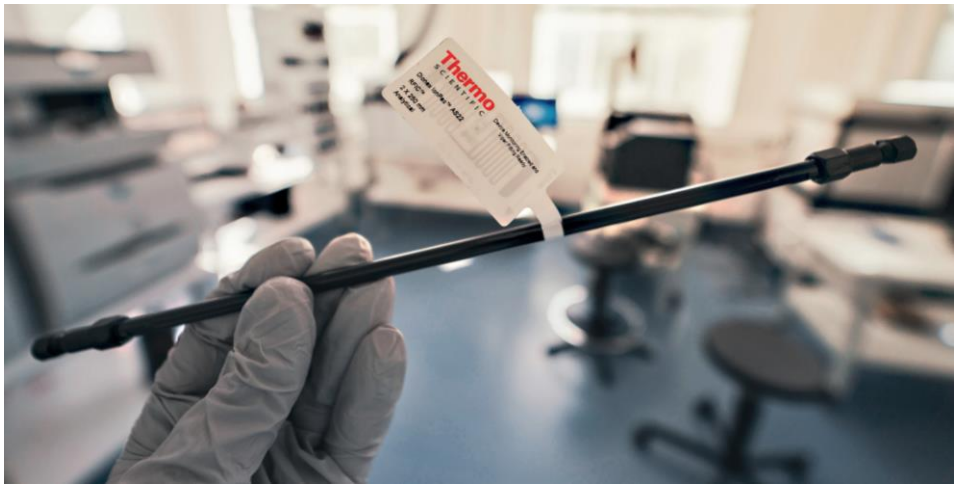

Figure 15: Thermo Scientific Dionex™ IonPac™ AS22

Sample preparation was carried out in an ISO class 8 clean room, while measurements were done in ISO class 7 to keep contaminations to a minimum. All solutions were prepared gravimetrically. Before weighing, the vessels were discharged with an antistatic gun Milty Zerostat 3 (Milty Media Care), in order to avoid electrostatic interferences. The weighing of the proteins and peptide standards was carried out using a microbalance Sartorius Cubis MSU 6.6 (Sartorius AG, Göttingen, Germany). For all other solutions and substances, the semi-micro balance CPA 225D (Sartorius AG, Göttingen, Germany) was used.

Evaporation during sample preparation was tested with two different systems, the Liebisch ™ Evaporator EVTF-130-36-16 (Gebr. Liebisch GmbH & Co. KG, Bielefeld, Germany) on the one hand and the GeneVac EZ-2 (SP Industries Inc., Warminister, USA) on the other. The centrifuge used was the Hermle Z 446K (HERMLE Labortechnik GmbH, Wehingen, Germany). For the heating process a thermomixer HLC MHR 13 (DITABIS Digital Biomedical Imaging Systems AG, Pforzheim, Germany) was used.

2.3 Cleaning procedures

In order to minimize sulfur contaminations, all consumables were subjected to a cleaning procedure. They were first treated with 10% HNO_3 for 24h, then with 1% HNO_3 for the same time and finally rinsed with ultrapure water. After drying in a fume hood, the consumables were stored in plastic bags. The HNO_3 was always replaced after multiple cleaning cycles. Glassware was avoided because of its high sulfur background. PFA or PP labware turned out to be better alternatives.

2.4 Sample preparation

2.4.1 Preparation of the solutions

- 25 mM NH_4Ac in ultrapure water, pH = 8.0 (1.9 mL NH_3 + 1.4 mL HAc + 996.7 mL H_2O)
- 250 mM NH_4Ac in ultrapure water, pH = 8.0 (18.8 mL NH_3 + 13.9 mL HAc+ 967.3 mL H_2O)
- 1% NH_4OH in ultrapure water, (0.4 mL NH_3 + 9.6 mL H_2O)
- 6M HCl in ultrapure water (1:1 dilution of HCl with H_2O)
- 1% HNO_3 in ultrapure water (15.3 mL HNO_3 + 984.7 mL H_2O)
- 10% HNO_3 in ultrapure water (153 mL HNO_3 + 847 mL H_2O)

2.4.2 Preparation of performic acid

The performic acid derivatization reagent was prepared by mixing 18 mL of formic acid, 2 mL of H_2O_2 and 100 µL of phenol and incubation for 30 min at room temperature until the typical yellow color of performic acid is reached (regarding practical handling smaller quantities of derivatization reagent can be prepared).

Since phenol is a solid at room temperature, it was slightly heated in a water bath (~ 60°C) to be pipetted. Formic acid was also be brought to a similar temperature to prevent the crystallization of phenol in the pipette tip.

2.4.3 Hydrolysis/ Oxidation of the proteins

1 mg β-Amyloid (the vial content) was mixed with 1 mL 1% NH_4OH. To dissolve the entire content, the solution was added via a syringe, which penetrates the membrane of the vial. After that a homogenization step was done, by sonication for 1 min. The solution was then aliquoted in 100 µL fractions and 3 of each peptide (Aβ40, Aβ42) were used, while the others were stored in a fridge. This procedure was necessary because the peptides could not be weighed in due to electrostatic interactions inside of the vial.

10 mg of the proteins (myoglobin, lysozyme) were solved in 2 mL of 0.9% NaCl and 3 aliquots were taken (each 40 µL). For NIST 2389a 4 fractions of the solution were directly weighed in (10µL).

Each of those fractions were spiked with 20 µL of the ^{34}S-enriched yeast hydrolysate. Subsequently 500 µL of performic acid were added and the samples were incubated at 65°C for 15 min. After that they were evaporated to dryness, mixed with 1 mL of 6M HCl and incubated again at 100°C for 24h.

The now oxidized and hydrolyzed samples were vortexed and centrifuged at 10000 rcf for 5 min. They were transferred to Eppendorf tubes, diluted 1:10 with the buffer (25 mM NH_4Ac) in HPLC vials and were directly used for analysis.

3. Results and discussion

3.1 Sulfur measurements

ICP-MS was the method of choice for the measurements because of its multi element capability, high sensitivity and wide dynamic range. For certain elements like sulfur, however, the instrument shows some limitations. This is mainly due to polyatomic interferences, which are created in the plasma from several isotopes of the matrix and superimpose the signal of other elements. Because of its low mass, sulfur is particularly susceptible to such interferences, with the $^{16}O_2^+$ ion being the most problematic one due to its abundance.

Table 10: Polyatomic interferences of the sulfur isotopes

Isotope	Abundance [%]	Polyatomic interferences
^{32}S	95.02	$^{16}O_2^+$, $^{14}N^{18}O^+$, $^{15}N^{17}O^+$, $^{14}N^{17}O^1H^+$, $^{15}N^{16}O^1H^+$, $^{14}N^{16}O^1H_2^+$
^{33}S	0.75	$^{15}N^{18}O^+$, $^{14}N^{18}O^1H^+$, $^{15}N^{17}O^1H^+$, $^{16}O^{17}O^+$, $^{16}O_2{}^1H^+$, $^{32}S^1H^+$
^{34}S	4.21	$^{15}N^{18}O^1H^+$, $^{16}O^{18}O^+$, $^{17}O_2^+$, $^{16}O^{17}O^1H^+$, $^{33}S^1H^+$

The most common form of mass analyser, the quadrupole, with its low resolution is unable to distinguish these interferences from other elements. To prevent this, either a high-resolution mass spectrometer (e.g. TOF, SF) or a collision/reaction cell is required. The triple quadrupole mass spectrometer (MS/MS) used here has the latter and allows the measurement of sulfur with oxygen as reaction gas. After selecting m/z = 32 in the first quadrupole, O_2 is added in the CRC and generates $^{32}S^{16}O^+$, which passes through the second quadrupole at m/z = 48, while the interfering polyatomic ions are lost.

Due to the comparatively high ionization energy of sulfur, its sensitivity is relatively low, which is why an optimization step with flow injection was first necessary. That is why all sulfur isotopes were measured in the available CRC modes (H_2, O_2) and optimized with manual tuning. Specifically, for the H_2 mode, the M^+ ion was selected without mass shift, while the MO^+ ion was taken for O_2, as they showed the best sensitivity in experiments, as can be seen in **Table 11**.

Table 11: Sensitivity of ^{32}S and its reaction products in different CRC modes [82]

Isotope	No gas [cps/ppb]	H_2 [cps/ppb]				O_2 [cps/ppb]			
		M^+	MH^+	MH_2^+	MH_3^+	M^+	MO^+	MO_2^+	MO_3^+
^{32}S	6181	4137	631	97	4	131	2038	2	0

The no gas mode was omitted for the reasons given above ($^{16}O_2^+$). Here, a series of standards in a concentration range of 0.1 - 100 µg L^{-1} was measured, as well as pure blanks (1% HNO_3) for the calculation of the LOQ. In addition, different materials such as quartz, PFA or PP were analysed for their sulfur background, before and after their purification with acids.

Table 12: List of experiments with different materials and cleaning procedures

Experiment number	PP	PFA	Quartz	Cleaned in HNO_3	Cleaned in HCl	Cleaned pipette tips (HNO_3)	Cleaned pipette tips (HCl)
1	x						
2		x					
3			x				
4	x			x			
5		x		x			
6			x	x			
7	x				x		
8		x			x		
9			x		x		
10	x			x		x	
11	x				x		x

As you can see in **Table 12** different combinations of materials and cleaning procedures were tried out to get as low a sulfur background as possible. However, there were no significant differences in the measurement as all values were below the LOQ and had similar CPS. One can therefore assume that at least for flow injection measurements with autosampler no improvement of the sulfur background can be achieved by pre-cleaning. Careful work in a clean room environment and pure chemicals seem to be enough to minimize sulfur contamination.

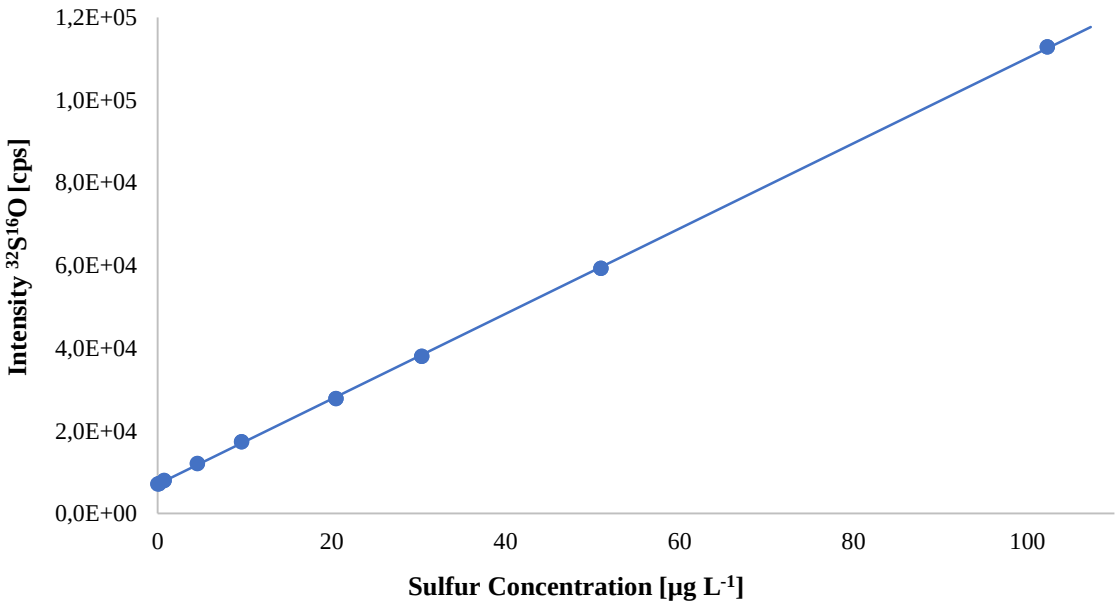

Figure 16: Calibration curve of sulfur (^{32}S → $^{32}S^{16}O$) in a concentration range of 0.1 – 100 µg L^{-1}

As also described in the literature, the O_2 mode achieved the best results. Here, good linearity over the entire concentration range of 0.1-100 µg L^{-1} could be shown, with an LOQ of 0.21 µg L^{-1}, which can be seen in **Figure 16**. The values were calculated by measuring a clean blank 10 times and using the following equation.

Equation 3: Calculation of the LOQ

$$LOQ = \bar{M}_{blank} + 10 \cdot \sigma_{blank}$$

$\bar{M}_{blank}$	Mean value of blank
σ_{blank}	Standard deviation of blank

In H_2 mode without mass shift, you could see good sensitivity, but the background is too high due to numerous interferences, which leads to unusable results.

Table 13: Parameters of the calibration curves in different CRC modes

	32 → 32 S [H_2]	32 → 48 S [O_2]	33 → 33 S [H_2]	33 → 49 S [O_2]	34 → 34 S [H_2]	34 → 50 S [O_2]	36 → 36 S [H_2]	36 → 52 S [O_2]
LOQ [µg L^{-1}]	N/A	0.2	N/A	7.3	N/A	1.9	N/A	N/A
Slope	N/A	1030.7	N/A	8.4	N/A	51.3	N/A	N/A
Intercept	N/A	7104.9	N/A	603.5	N/A	384.1	N/A	N/A
RSQ	N/A	0.9999	N/A	0.9989	N/A	0.9999	N/A	N/A

The data shown in **Table 13** refers to the measured sulfur standard, which has a natural isotopic distribution, thus, resulting in worse values for the less abundant isotopes like ^{33}S. Nevertheless, it is important to look at the LOQ values in this context, because for isotope dilution, all sulfur isotopes in the peptides must be measured. It was possible to measure 3 of the sulfur isotopes in O_2 mode with excellent R^2 values. Unfortunately, ^{36}S could not be measured at the present concentrations because it only has a natural abundance of 0.02%.

Table 14: Natural isotopic composition of sulfur

Isotopic abundance [%]			
^{32}S	^{33}S	^{34}S	^{36}S
95.02	0.75	4.21	0.02

3.2 Development of the amino acid separation

3.2.1 Characteristics of the sulfur-containing amino acids

In order to separate the sulfur containing amino acids with an HPLC, one has to take advantage of their characteristic properties. In particular, two separation techniques are in focus: anion exchange and reversed phase chromatography. The separation of the first method is based on the fact that cysteine forms more negatively charged ions in a basic environment due to the lower pKa value at C_α-COOH, resulting in a longer retention time in the positively charged column (e.g. DEAE resin). Reversed phase, on the other hand, utilizes hydrophobic interactions of the analyte with a mostly silica-based stationary phase to cause separation. Here, methionine should elute later than cysteine

due to its higher hydrophobicity. The value given in **Table 15** refers to the "transmembrane tendency" hydrophobicity scale. [83]

There are many different scales describing the hydrophobic behavior of amino acids. The one above was used because it is relatively new, compared to the Kyte and Doolittle scale, and in agreement with most other ones, that methionine is more hydrophobic.

Table 15: Characteristics of the sulfur containing amino acids

Amino acid	1-letter code	pKa C_α-COOH	pKa C_α-NH_3^+	pKa side chain	tt Hydrophobicity
Cysteine	C	1.71	10.78	8.33	-0.3
Methionine	M	2.28	9.21	-	1.4

For the oxidized forms of these amino acids, methionine sulfone and cysteic acid, no conclusive date was found in literature. Nevertheless, it can be estimated from their molecular structure that they have a higher charge and lower hydrophobicity because of the additional oxygen.

3.2.2 Separation by reversed phase chromatography

Initial test measurements were performed with a reversed-phase column, the Atlantis T3. For this purpose, different standards of amino acids and sulfate were measured to see whether a separation is possible. After some isocratic measurements, a gradient of NH_4Ac and MeOH was created, which was gradually optimized, to get fast and accurate separation. The use of MeOH reduces the polarity of the eluent, which causes the more hydrophobic substances to elute faster from the column. The final gradient is shown below in **Table 16**.

Table 16: Gradient for the reversed phase chromatography

HPLC conditions	
Column	Atlantis T3
Buffer A	10 mM NH_4Ac, pH = 5
Buffer B	MeOH
0 – 1 min	100% A
1 – 5.5 min	Ramp to 20% B, 80% A
5.5 – 6 min	20% B, 80% A
6 – 6.05 min	Ramp to 100% A
6.05 – 7 min	100% A

Unfortunately, complete separation could not be achieved, as you can see in the following chromatogram.

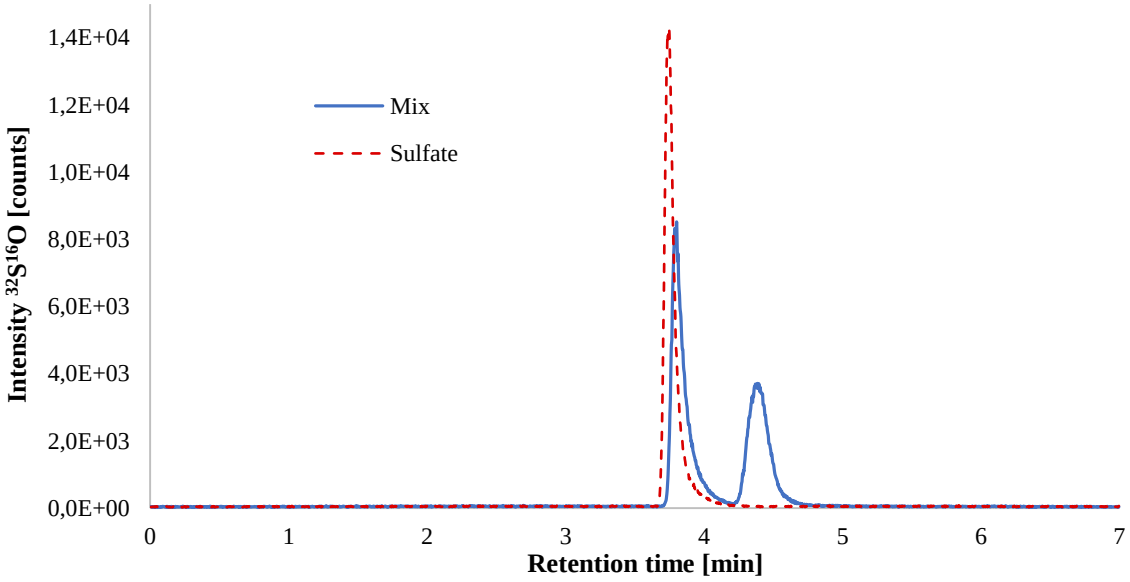

Figure 17: Chromatogram of a 2 mg L^{-1} amino acid mixture containing methionine, cysteine and their oxidized forms with a 500 µg L^{-1} sulfate standard in the background

The separation of cysteine (RT = 3.79 min) and methionine (RT = 4.39 min) was possible, however they showed an overlap with their oxidized forms. In addition, evaluation of cysteine was difficult because sulfate had a very similar retention time of 3.74 min. Although only methionine is required for the quantification of Aβ peptide, it was not possible to see whether the oxidation in

the sample preparation was complete, which is why the results were seen as insufficient. Therefore, in the following measurements, an anion exchange column was used, the Dionex™ IonPac™ AS22.

3.2.3 Separation by anion exchange chromatography

The aim of the optimization was to develop the shortest possible method by which cysteine, methionine and their oxidized forms as well as sulfate can be well separated from each other. In addition to a good quantification of the peptides, this separation also shows whether the oxidation in the sample preparation was complete. For this, first isocratic elution was tested at different NH_4Ac concentrations to see when the respective substances elute. The expected behavior of the amino acids could be confirmed here with standards. Methionine and methionine sulfone eluted at 20 mM NH_4Ac, cysteine and cysteic acid at 100 mM NH_4Ac, and sulfate required 400 mM NH_4Ac to get an acceptable retention time. Based on this knowledge an attempt was made to create a suitable gradient.

Table 17: Gradient for the anion exchange chromatography

HPLC conditions	
Column	Dionex™ IonPac™ AS22
Buffer A	20 mM NH_4Ac, pH = 8.0
Buffer B	400 mM NH_4Ac, pH = 8.0
0 – 4 min	100% A
4 – 7 min	Ramp to 100% B
7 – 12 min	100% B
12 – 12.1 min	Ramp to 100% A
12 – 16 min	100% A

In **Table 17** you can see the optimized parameters of the gradient. It was important to ensure that the peaks elute within isocratic steps, as the sulfur background increases with higher salt concentration and this could have an impact on the ID measurements. In order to avoid an overlap of methionine and methionine sulfone the gradient started isocratic at low concentration. With 20mM NH_4Ac optimal separation could be achieved within 4 min. Directly after the methionine sulfone peak, the concentration was then rapidly increased (400 mM NH_4Ac) to elute the

remaining peaks as quickly as possible. The increase was gradual over 3 minutes to ensure a stable eluent for the next isocratic step. Due to their strong negative charge, cysteine, cysteic acid and finally sulfate only elute after 10 min. After the elution of all the analytes, the gradient was changed back to the starting conditions (20 mM NH_4Ac) and left for additional 4 minutes to equilibrate the system for the next measurement. This last step is very important because without equilibration, the following sample can elute early, resulting in overlapping peaks and new retention times.

To test the developed method, a mixture of the amino acids, their oxidized forms and sulfate was prepared. In order to obtain a good comparison of the peaks, the concentration of the analytes was adjusted so that they each contained approximately 100 µg L^{-1} of sulfur.

Figure 18 shows the chromatogram of this test measurement together with the optimized gradient. All analytes were successfully separated within the measuring time of 16 min. The 4 min equilibration time led to reproducible results. In several measurements, the same chromatograms were obtained without retention time shifts.

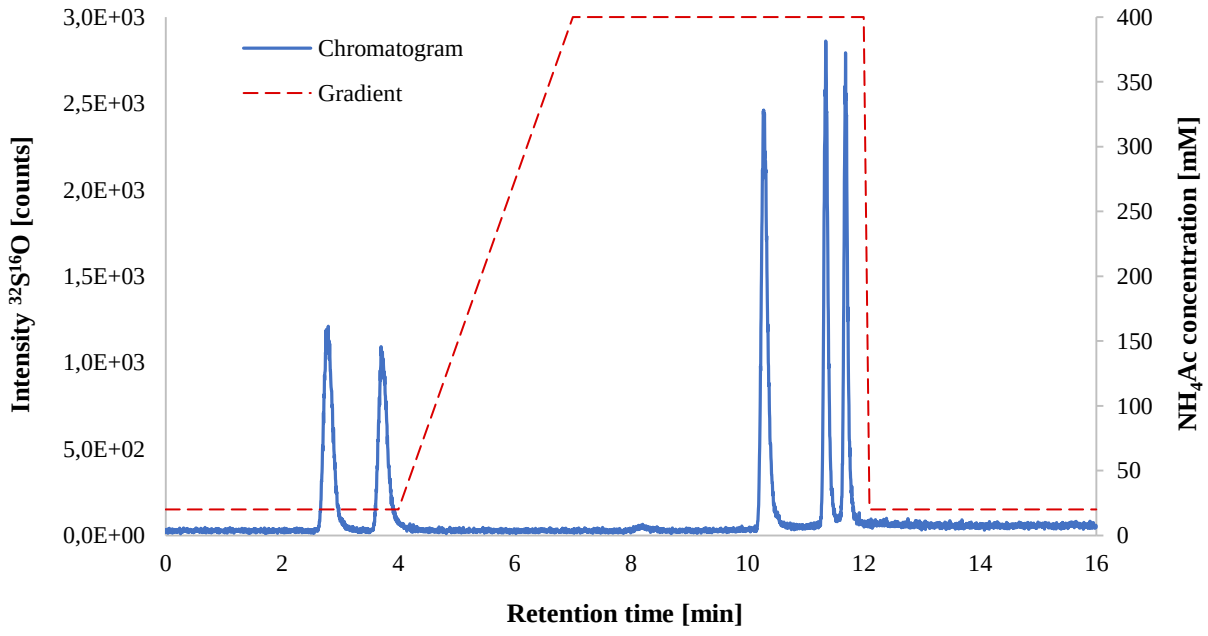

Figure 18: Chromatogram of a 100 µg L^{-1} (sulfur concentration) amino acid mixture containing methionine, cysteine and their oxidized forms in addition to sulfate with the optimized HPLC gradient in the background

Using this gradient, calibration curves of the individual standards were then created in a concentration range of 50-1000 µg L^{-1} and the LOQ values determined by means of a clean blank, again calculated with **Equation 3.** For the LOQ of sulfate, simply the peak areas of the blank were used. However, since no peaks were visible for the amino acids, the counts around their retention times had to be employed. Accordingly, cysteic acid has a higher LOQ value because the sulfur background at 400mM NH_4Ac is slightly higher.

Table 18: Parameters of the amino acid measurements

Substance	Retention time[min]	LOQ Substance [µg L^{-1}]	LOQ ^{32}S [µg L^{-1}]
Methionine	2.77	6.6	1.4
Methionine sulfone	3.30	9.5	1.7
Cysteine	10.27	5.8	1.5
Cysteic acid	11.35	12.1	2.3
Sulfate	11.69	-	9.8

Compared to inorganic sulfate, the amino acids can be measured with better sensitivity, since they are less prone to suffer from contaminations. Therefore, they can be measured over a wide concentration range with excellent linearity, as shown in **Figure 19**.

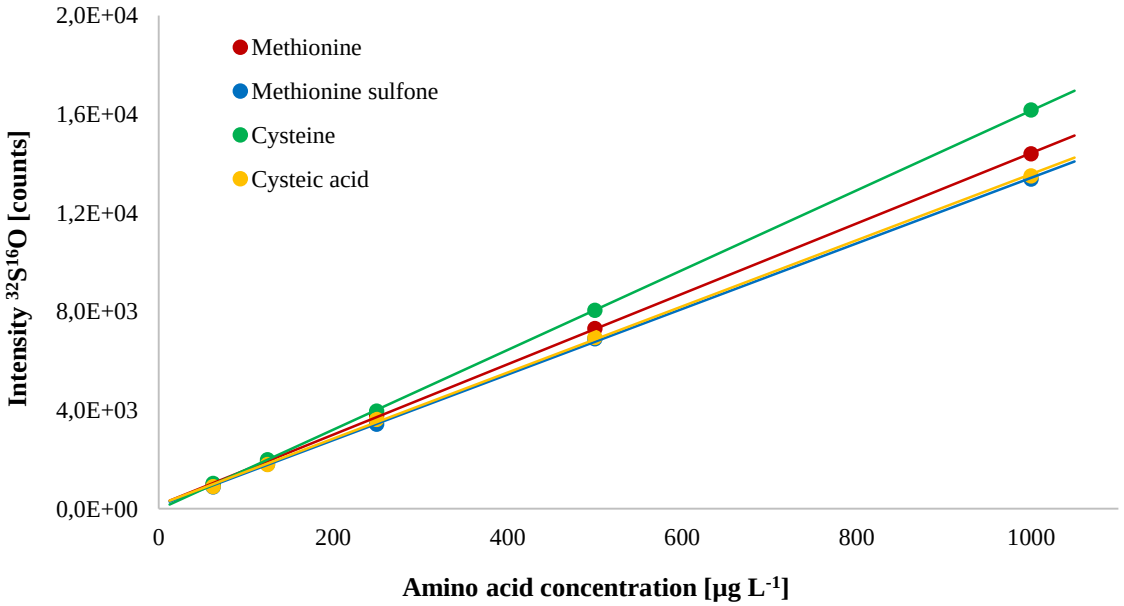

Figure 19: Calibration curves of the amino acids in a concentration range of 50-1000 µg L^{-1}

3.2.4 Colum cleaning procedures

A problem of the strong anion exchange column was that the inorganic sulfate elutes very late due to its strongly negative charge and often accumulates in the column at higher concentrations. Although sulfate itself is not required for the quantification of the peptides, it may overlap with the peak of cysteic acid because of their similar retention time, making evaluation difficult. After many measurements with sulfate standards, contaminations in a range of 10-100 µg L^{-1} are possible.

To remove them, high concentrations of the eluent (400 mM NH_4Ac) were injected into the column for a long time (1-2 h), but unfortunately this did not lead to an improvement of the background. In addition, higher pH (pH 10-11) values were tried to completely dissociate the acetate and create more competing ions, but this led to the same results. In the end, a stronger clean-up solution was chosen, 200 mM HCl in 80% ACN, which is recommended by the manufacturer for ionic and hydrophobic contaminations. The acidic environment causes a suppression of ionization and ion exchange interactions, thus removing the sulfate from the resin and solving it in an organic solution.

For this, the column was first rinsed with ultrapure water for several minutes, then with the clean-up solution for 1 h, subsequently again with water for 1-2 h and finally with the eluent for 30 min. This reduced the sulfate background by 92% (**Figure 20)** The long rinsing process at the end was of great importance, as the plasma becomes unstable, when injecting organic solutions, if the ion optics are not exchanged previously. Even small quantities of ACN can cause a shut-down of the plasma. In order to avoid decomposition of ACN in the acidic solution, the clean-up solution should always be prepared immediately before use.

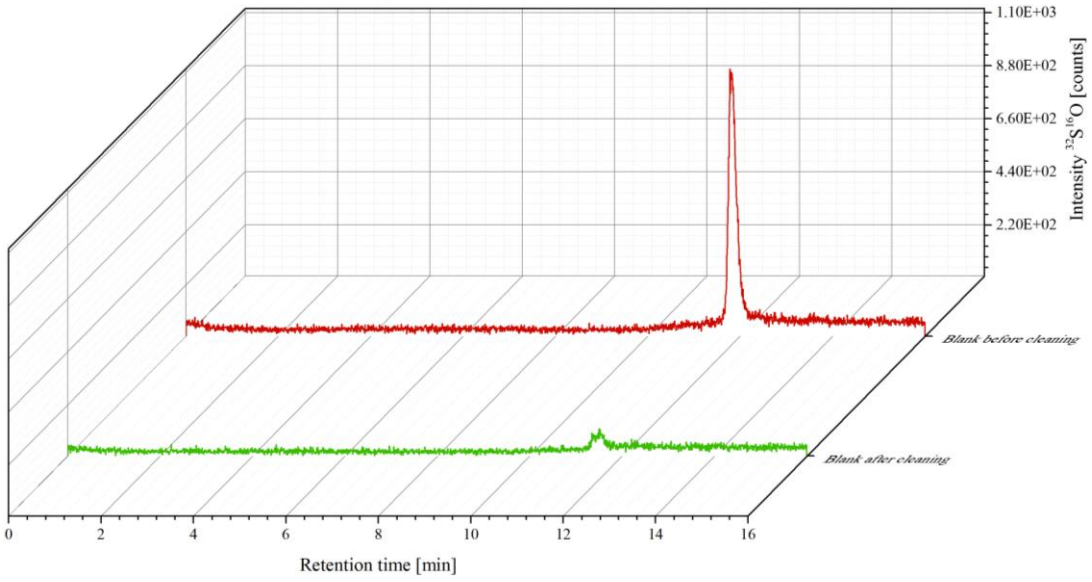

Figure 20: Comparison of the sulfate background before and after using 200 mM HCl in 80% ACN

In addition to the column, the injection needle of the HPLC is also a major source of contamination. Normally it is washed out between measurements with isopropanol, but this is not suitable for every substance. Within these measurements, blanks showed clear traces of the sulfur-containing amino acids cysteine and methionine, which means that IPA was not enough. That is why wash vials were used for cleaning, into which the needle enters 5 times after each measurement. As cleaning solutions, 400 mM NH_4Ac, 10% MeOH and 20% MeOH were tested. The methanol mixtures both showed excellent results, with the amino acids being successfully removed. For this reason, 10% MeOH was used for all further measurements, since this concentration was already sufficient.

3.3 Separation of the protein standards

3.3.1 Characteristics of the proteins/peptides

Since the peptide quantification is dependent on the sulfur-containing amino acids, the quality of the measurement is significantly influenced by the proportion of methionine and cysteine within the sequence. Even though Aβ only contains 1 methionine, the total mass is significantly lower than that of the other proteins, which leads to increased sensitivity. Nevertheless, lysozyme is of course better to measure because it contains both amino acids in large quantities, which also allows two peaks to be used for quantification. In addition, it must also be considered that the Aβ is much

more expensive due to the synthetic production and therefore sold in smaller quantities (0.1-1 mg), which is why you have to work with lower concentrations.

Table 19: Important parameters of the investigated proteins/ peptides

Protein/peptide	Molecular structure	Mass [Da]	Sequence length	Sulfur containing amino acids
β-Amyloid 40/ 42		4331.50/ 4514.10	672-711/ 713	1 Methionine
Lysozyme from chicken egg white	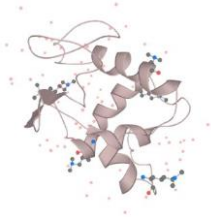	14313.14	19-147	2 Methionine, 8 Cysteine
Myoglobin from equine skeletal muscle	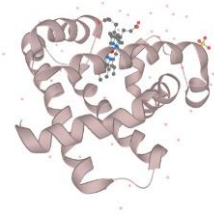	17015.48	2-154	2 Methionine

3.3.2 Analysis of the standards via HPLC-ICP-MS/MS

Using the optimized gradient, the protein and peptide standards were now separated chromatographically. In addition to Aβ40 and Aβ42, the proteins myoglobin and lysozyme as well as the standard reference material NIST 2389a were measured. The latter is an amino acid mix, containing cysteine and methionine in a similar concentration (~ 2.5mmol / L). The ^{34}S-enriched yeast hydrolysate was also analysed to characterize its composition.

All samples were exposed to full hydrolysis/oxidation prior to analysis and were further diluted 1:10 with 25 mM NH_4Ac, as described in the method section. However, two different evaporation systems were used, which had a significant impact on the results.

Evaporation with GeneVac EZ-2:

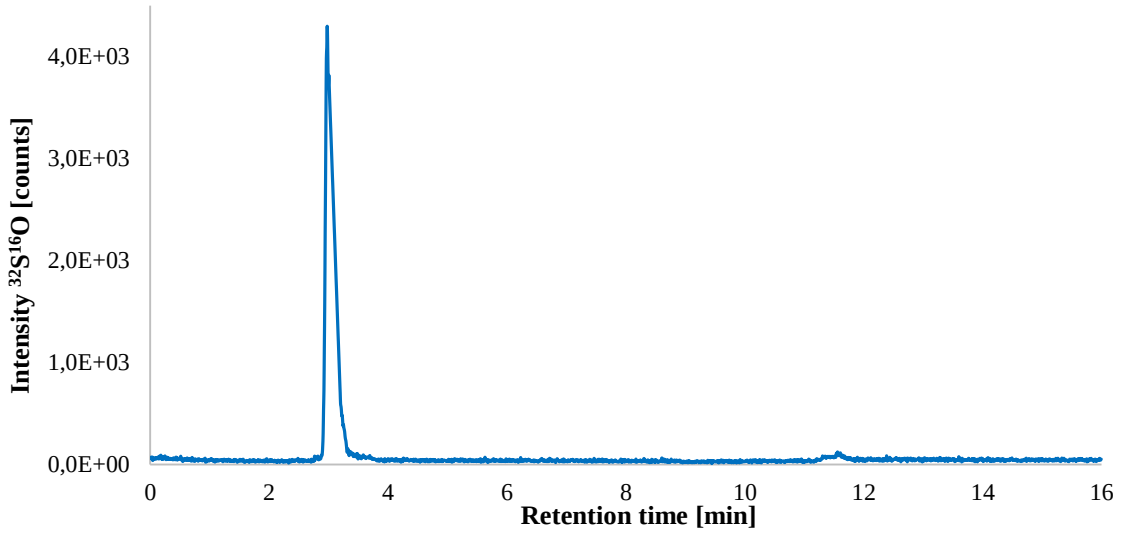

Figure 21: Chromatogram of Aβ40 after hydrolysis/oxidation using HPLC-ICP-MS/MS (~ 10 mg L^{-1})

As was to be expected, only one peak at 3.3 min is visible for Aβ40, which corresponds to methionine sulfone. The amino acid thus appears to have been almost completely oxidized, which shows that the sample preparation was successful. A slight increase in intensity is only noticeable at 11.7 min because of the sulfate background. Aβ42 showed an identical pattern, but the area of methionine sulfone was significantly smaller (approximately 2.5 times) despite the same dilution, leading to a noisier chromatogram.

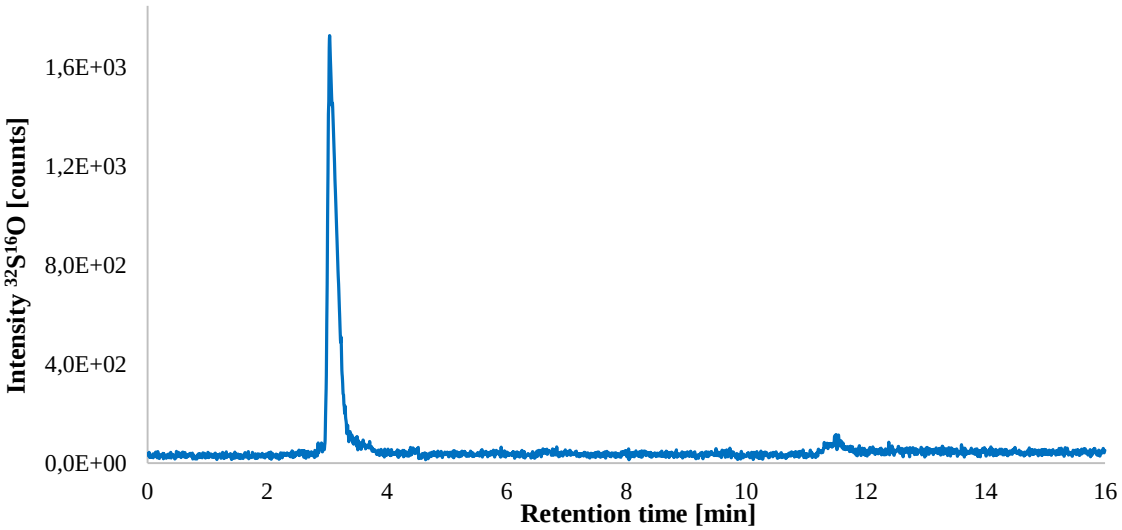

Figure 22: Chromatogram of Aβ42 after hydrolysis/oxidation using HPLC-ICP-MS/MS (~ 10 mg L^{-1})

Since lysozyme contains 2 methionine and 8 cysteine, the sensitivity is comparatively high, and two peaks can be seen at 2.3 and 11.3 min for their respective oxidized forms. The ratio of the peak areas is in good agreement with the number of sulfur-containing amino acids (2:8).

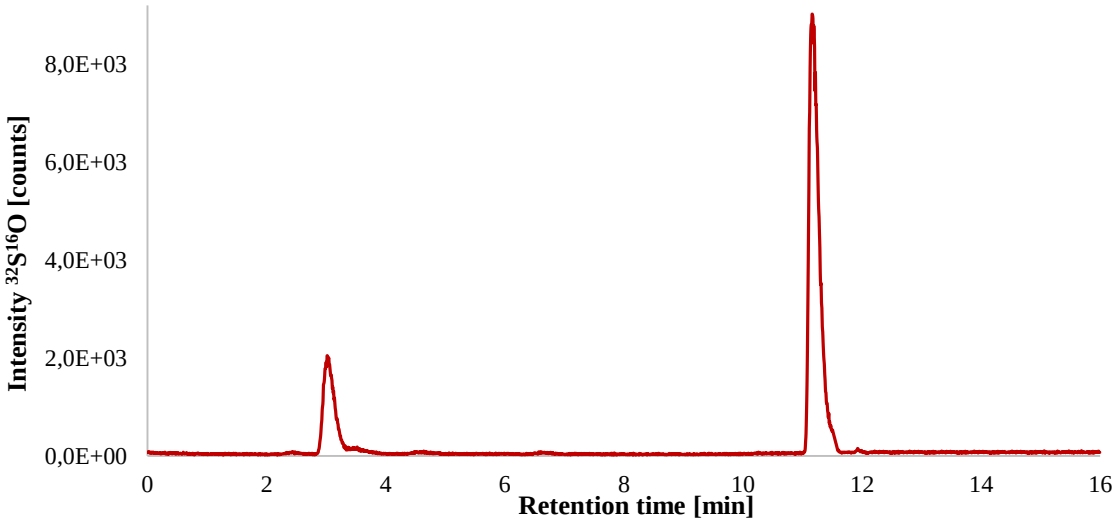

Figure 23: Chromatogram of lysozyme (VETRANAL) after hydrolysis/oxidation using HPLC-ICP-MS/MS (~ 20 mg L^{-1})

For myoglobin, on the other hand, the chromatogram looks very similar to the Aβ peptides, since there are only 2 methionine molecules in the sequence. Due to the small peak at 6.4 min, it can be assumed that slight contamination with cysteine may have occurred.

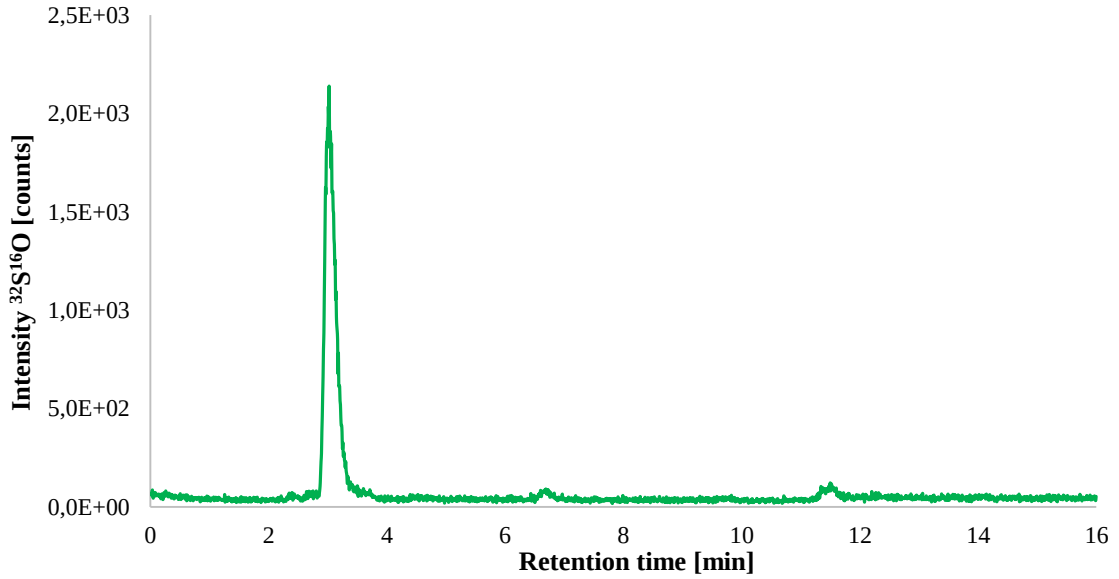

Figure 24: Chromatogram of myoglobin (≥98%) after hydrolysis/oxidation using HPLC-ICP-MS/MS (~ 20 mg L^{-1})

The similar concentrations of methionine and cysteine in the NIST 2389a standard resulted in two peaks with almost identical area. However, a small part of the cysteine can also be found in its unoxidized form.

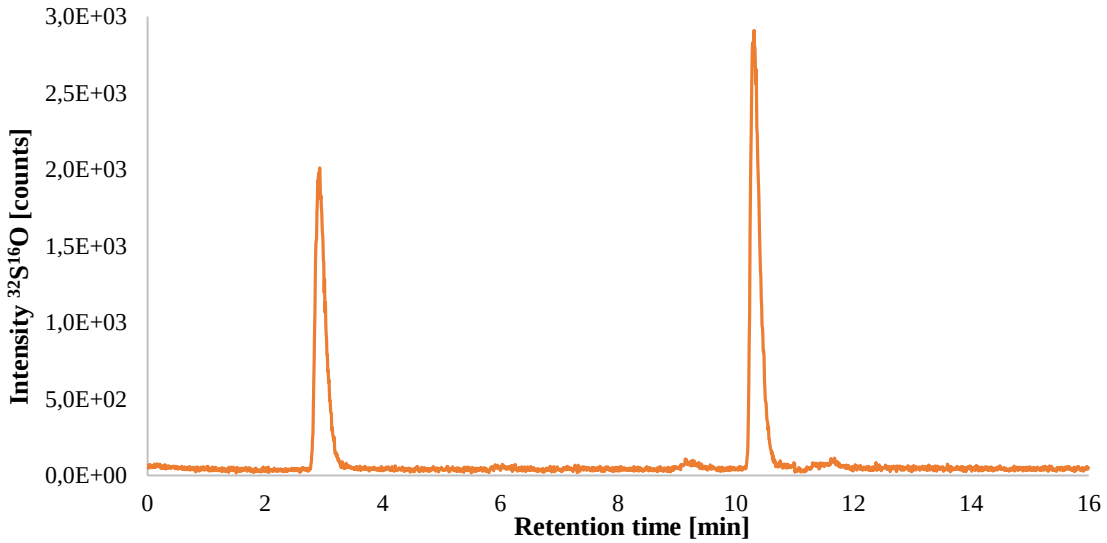

Figure 25: Chromatogram of NIST 2389a SRM after hydrolysis/oxidation using HPLC-ICP-MS/MS (~ 1:200 dilution)

For the yeast, it was necessary to measure ^{34}S because of its role as a spike. Numerous peaks can be seen in the hydrolysate, with methionine sulfone, cysteic acid and sulfate having the largest area. The others are presumably derivatives of amino acids and various forms of inorganic sulfur (e.g. SO_3^{2-}).

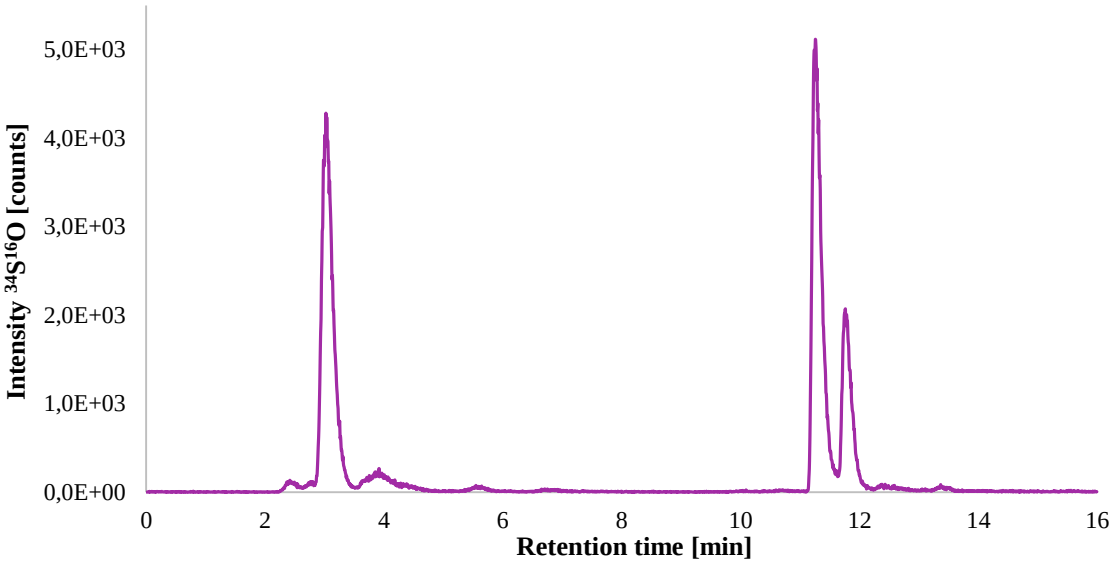

Figure 26: Chromatogram of the ^{34}S-enriched yeast hydrolysate using HPLC-ICP-MS/MS (1:100 dilution)

Evaporation with Liebisch ™ Evaporator EVTF-130-36-16:

This system turned out to be unsuitable for the sample preparation. Since the evaporation was heat-assisted, adducts seem to have formed from the amino acids, making evaluation difficult. In addition, the blowing of nitrogen through capillaries led to further contaminations, mainly inorganic sulfur compounds, since the retention times were very high (~ 11-13 min).

In order to show the effects of this method on the sample, the chromatograms of both systems were compared below. Only one of the β-amyloid peptides was shown here, since their chromatograms looked almost identical.

Instead of methionine sulfone at 3.3 min, a peak with a similar area is visible at 2.5 min, which corresponds more to the unoxidized form. However, this peak is also overlaid with a smaller one, which could be another substance.

For cysteine, it is difficult to say which adducts may have formed because the retention time has shifted massively. There is a very broad peak at 4.9 min along with a small one at 6 min.

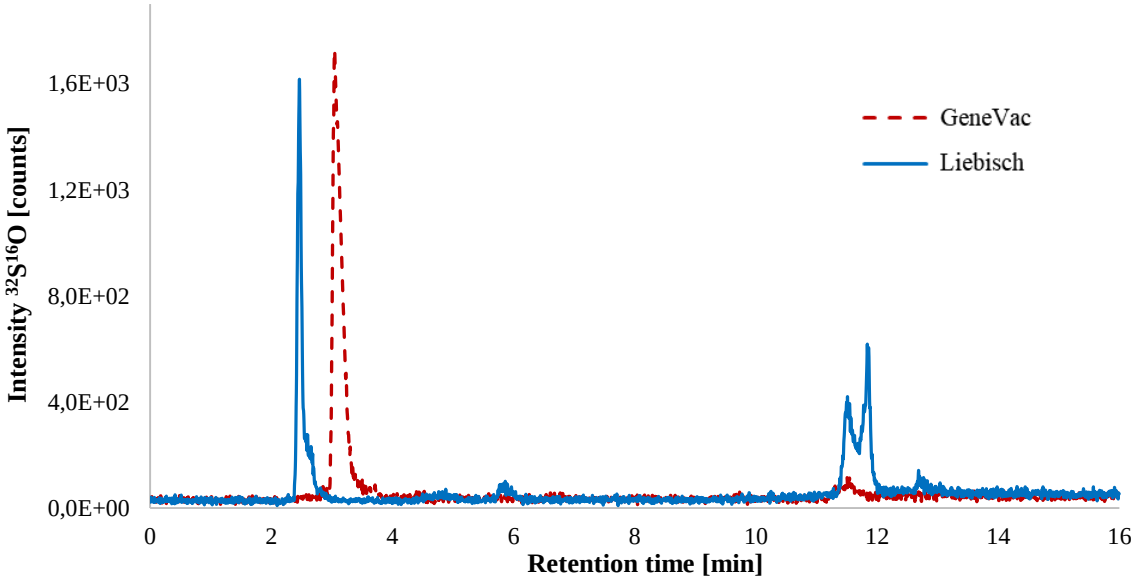

Figure 27: Comparison of the chromatograms for Aβ40 with different evaporation methods (~ 10 mg L^{-1})

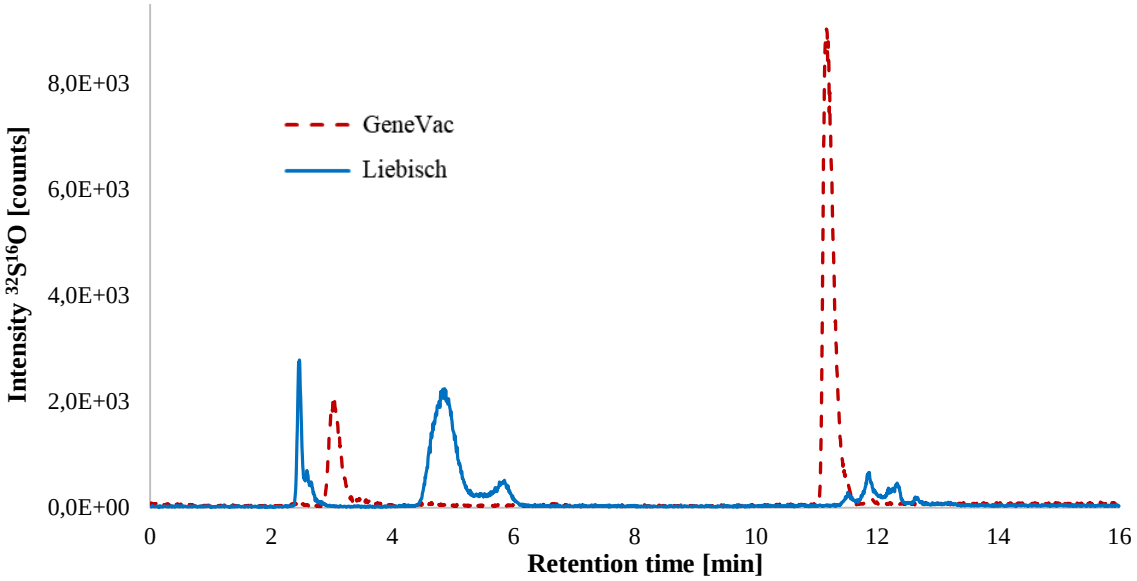

Figure 28: Comparison of the chromatograms for lysozyme with different evaporation methods (~ 20 mg L^{-1})

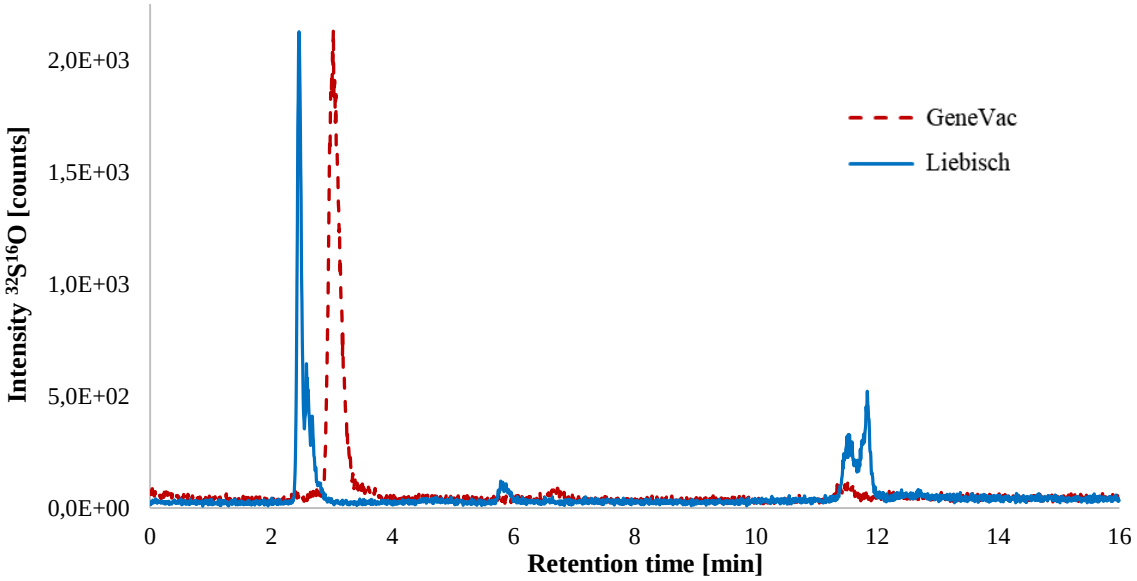

Figure 29: Comparison of the chromatograms for myoglobin with different evaporation methods (~ 20 mg L^{-1})

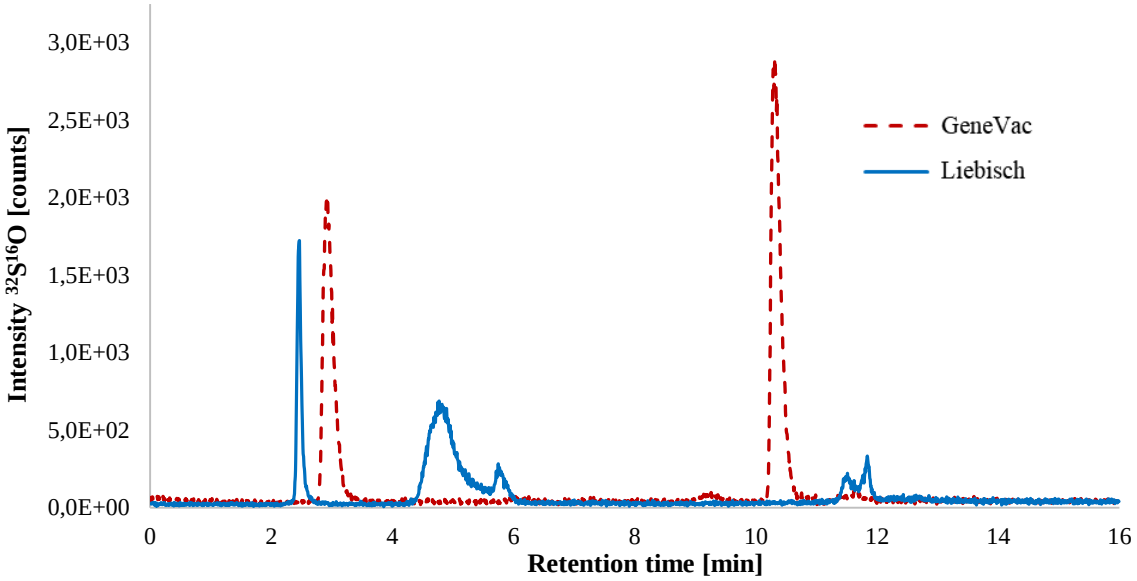

Figure 30: Comparison of the chromatograms for NIST 2389a with different evaporation methods (~ 1:200 dilution)

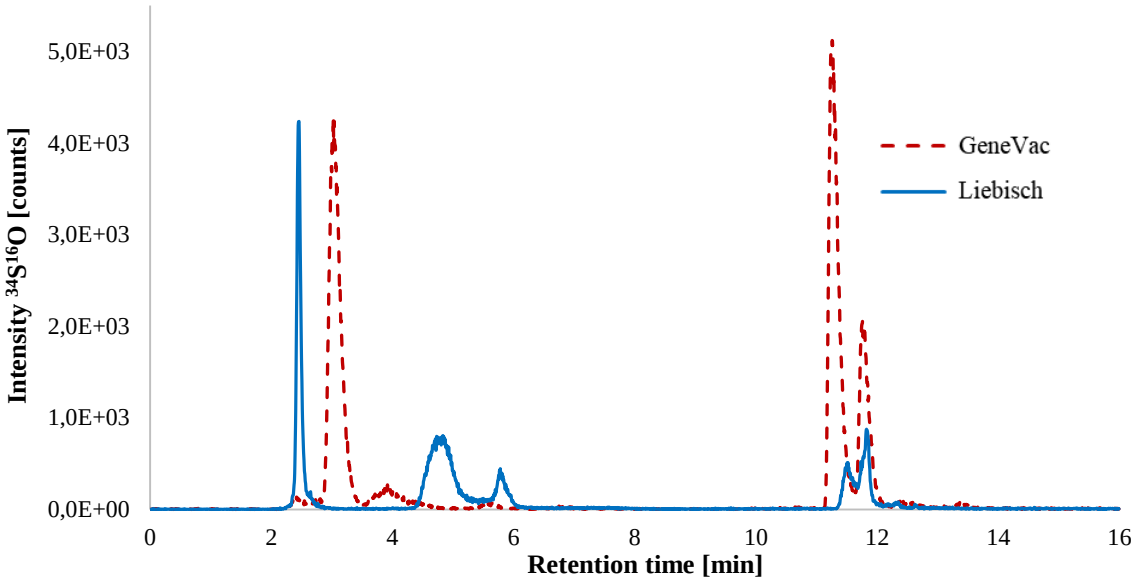

Figure 31: Comparison of the chromatograms for the ^{34}S-enriched yeast hydrolysate with different evaporation methods (1:100 dilution)

3.4 Quantification of the peptide content

3.4.1 External calibration with ^{34}S standard

In order to compare the different quantification methods with each other, external calibration was first tested. However, a ^{34}S-enriched sodium sulfate standard (>98%) was used, as this means that sulfate contamination could be neglected due to the low natural abundance of ^{34}S. For this purpose, a series of dilutions was set up in the concentration range of 20-200 µg L^{-1}.

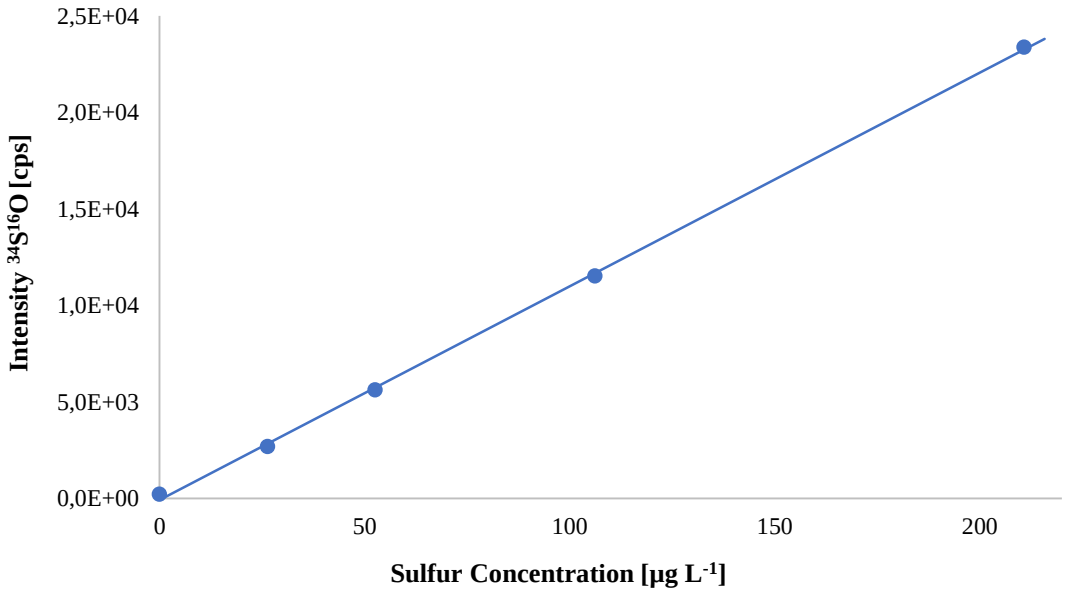

Figure 32: Calibration curve of sulfur (^{34}S → $^{34}S^{16}O$) in a concentration range of 20 – 200 µg L^{-1}

As was to be expected, the calibration curve showed good linearity over the entire concentration range due to the low ^{34}S background.

Table 20: Parameters of the ^{34}S calibration curve

	Slope	Intercept	RSQ
^{34}S	110.7	84.0	0.9995

The quantification was then carried out by integrating the ^{32}S peaks of the oxidized amino acids and inserting the values into the ^{34}S calibration curve, taking into account the different abundances of the isotopes (^{32}S = 95%, ^{34}S = 98%). Procedural blanks (20 mM NH_4Ac) were used for correction. By comparing these values with the theoretical ones, the purity of the standards could

be determined. 3 replicates were measured for each of the samples and 4 for NIST 2389a. Based on the recovery of this standard reference material, a verdict could already be made about the accuracy of the method.

Since only 66% of the mass fraction was recovered for cysteine and 70% for methionine, around 30 - 40% seem to have been lost during sample preparation. This is very plausible since the samples were transferred to new vessels in several steps and were exposed to many processes such as heating or vaporization.

Table 21: Measured mass fractions of the SRM in comparison with the certified values (external calibration)

Amino Acid	Certified mass fraction [mg g^{-1}]	Measured mass fraction [mg g^{-1}]	Recovery [%]
Cysteine	0.295 ± 0.013	0.195 ± 0.02 (n=4)	66.12 ± 0.06
Methionine	0.373 ± 0.011	0.260 ± 0.02 (n=4)	69.73 ± 0.05

Because of these losses, the percentage peptide content of the standards was also very low, between 50 and 60% and the values could not be used for the purity determination. However, there were also noticeable differences between the standards.

The peptide content of the proteins myoglobin and lysozyme was increased with a higher degree of purity in the standard. In addition, you can see again, as in the previous measurements, that Aβ40 had 2.5 times more peptide content than Aβ42.

Table 22: Determined peptide content of the different standards (external calibration)

Peptide content [%]		
Myoglobin (95-100%)	53.05 ± 1.02	n = 3
Myoglobin (≥98%, SDS-PAGE)	59.06 ± 3.75	n = 3
Lysozyme (≥90%)	59.29 ± 5.52	n = 3
Lysozyme (VETRANAL)	61.54 ± 5.33	n = 3
Amyloid β 1-40 (98%)	49.19 ± 3.22	n = 3
Amyloid β 1-42 (>97%)	19.99 ± 1.71	n = 3

3.4.2 Post column on-line isotope dilution

By adding the ^{34}S spike post column, on-line isotope dilution was also tested for quantification. However, this method suffered from the same problems as external calibration because errors in sample preparation are not taken into account. Accordingly, the results looked very similar here, making further measurements unnecessary. In addition, there were frequent irregularities in the peristaltic pump, making evaluation difficult.

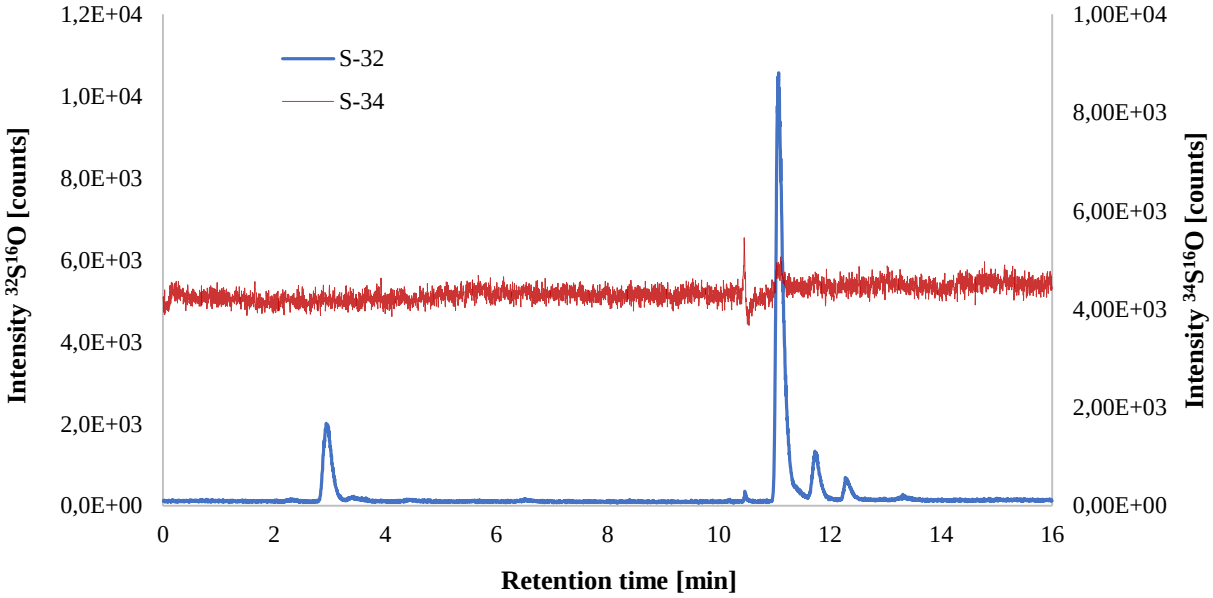

Figure 33: $^{32}S/^{34}S$ Chromatogram of lysozyme using on-line isotope dilution

3.4.3 Procedure of the species-specific isotope dilution

In order to ensure traceability with this type of isotope dilution, each standard must be quantified step by step. Therefore, first the ^{34}S spike had to be measured precisely using reverse isotope dilution. The term reverse here refers to the characterization of the spike instead of the sample. After that the two standards of the oxidized amino acids (methionine sulfone, cysteic acid) were determined using this spike. By adding these standards to the^{34}S-labelled yeast hydrolysate, its composition could be characterized using the anion exchange column.

Only after these steps was it possible to add the yeast to the proteins during sample preparation. The following table provides an overview of the measurements required.

Table 23: Overview of the measurements required for species-specific isotope dilution

RIDMS of ^{34}S spike with certified ^{32}S standard by flow injection

↓

IDMS of cysteic acid, methionine sulfone with ^{34}S spike by flow injection

↓

Species-specific RIDMS of ^{34}S-labelled yeast hyrdosylate with cysteic acid, methionine sulfone by HPLC-ICP-MS/MS

↓

Species-specific IDMS of β-Amyloid with ^{34}S-labelled yeast hyrdosylate by HPLC-ICP-MS/MS

3.4.4 Characterization of the ^{34}S-labeled yeast hydrolysate

To characterize the ^{34}S-enriched yeast hydrolysate, a mixture was prepared together with the already quantified amino acid standards. In order to ensure well matched concentrations for the RIDMS, first test measurements with only yeast were done. Since many unknown small peaks were visible in the chromatogram and the sulfate overlapped with the cysteic acid, the gradient was slightly changed for yeast to get a better separation. The best results were obtained by using 40 mM instead of 20 mM NH_4Ac (buffer A). Starting with higher concentration leads to a faster equilibration at 400 mM NH_4Ac, thus shortening the retention time of cysteic acid, as you can see in **Figure 34**.

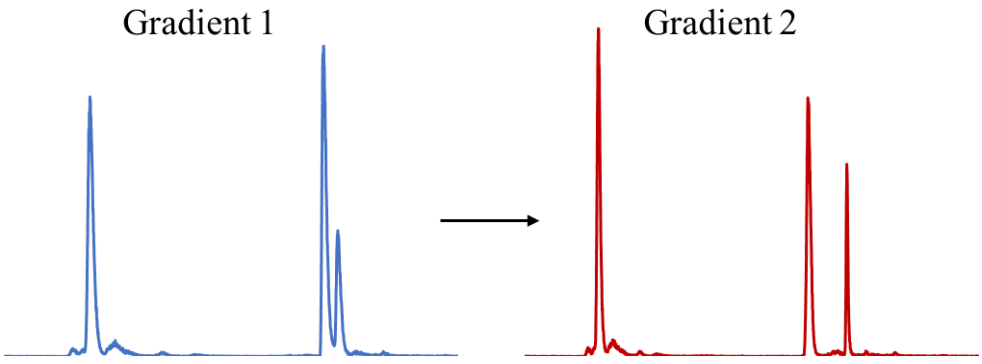

Figure 34: Chromatogram of ^{34}S-enriched yeast hydrolysate with 20 mM NH_4Ac (Gradient 1) and 40 mM NH_4Ac (Gradient 2) as buffer A

The yeast hydrolysate was measured a total of 10 times to allow accurate quantification. Methionine sulfone, cysteic acid and sulfate were the main components (containing sulfur). Other peaks were seen but they were all under the LOQ.

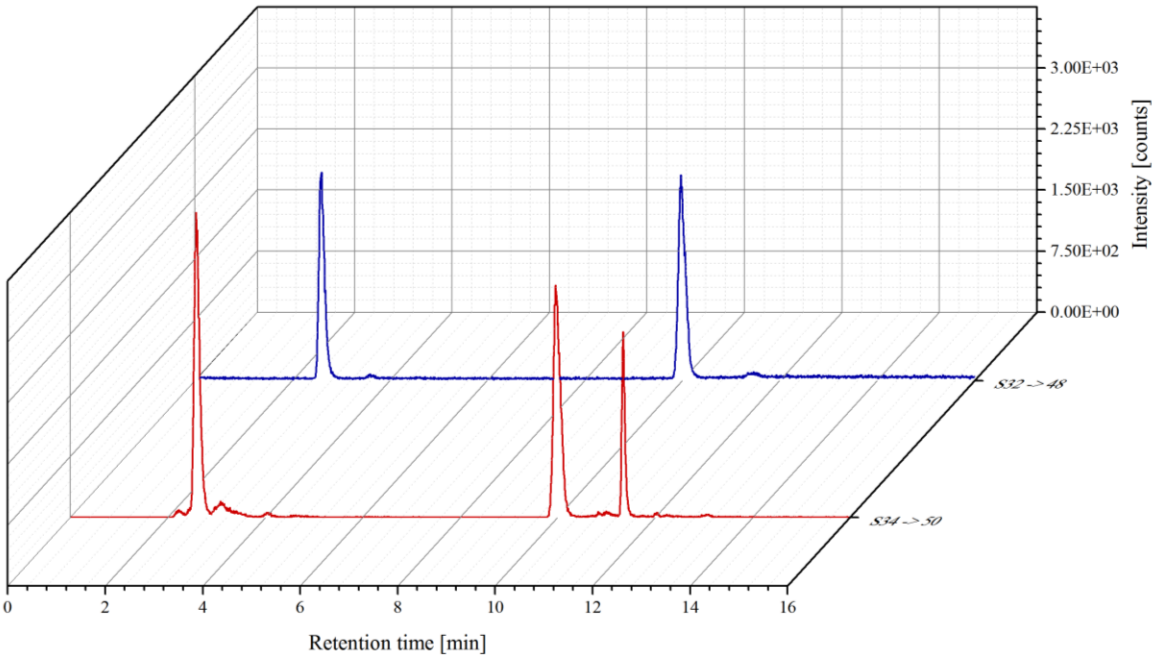

Figure 35: ^{32}S and ^{34}S chromatograms of the yeast mixture used for RIDMS

The two amino acids showed similar concentrations, smaller amounts of inorganic sulfate were also present. **Equation 1** was used for the calculation.

Table 24: Concentrations of the sulfur containing components in the yeast hydrolysate

Substance	Mass fraction [mg g^{-1}]
Methionine sulfone	6.65 ± 0.04 (n=10)
Cysteic acid	5.49 ± 0.04 (n=10)
Sulfate	0.42 ± 0.01 (n=10)

The isotopic distribution within the yeast itself was also of great importance. No ^{32}S peaks were detected, which was beneficial for the IDMS measurements. Only small quantities of ^{33}S were seen.

Table 25: Sulfur isotope distribution in the ^{34}S-labeled yeast hydrolysate

Isotopic abundance [%]			
^{32}S	**^{33}S**	**^{34}S**	**^{36}S**
< LOD	1.02	98.89	< LOD

3.4.5 Quantification via species-specific isotope dilution

To certify the used procedure, 4 fractions of NIST 2389a were subjected to the same sample preparation and subsequently measured 2 times each.

Table 26: Measured mass fractions of the SRM in comparison with the certified values (species-specific ID)

Amino Acid	Certified mass fraction [mg g^{-1}]	Measured mass fraction [mg g^{-1}]	Recovery [%]
Cysteine	0.295 ± 0.013	0.297 ± 0.01 (n=8)	100.68 ± 1.69
Methionine	0.373 ± 0.011	0.368 ± 0.01 (n=8)	98.66 ± 3.22

The certified values were in good agreement with the measured ones, whereby a recovery of almost 100% for cysteine and 99% for methionine was achieved. Based on these results, it can be concluded that, in contrast to external calibration and on-line ID, which both suffered from bad recoveries, losses during sample preparation were compensated, making this method suitable for quantifying peptides in a reproducible manner.

The peptide content was determined by comparing the theoretical value with the measured one. Since the Aβ cannot be weighed accurately due to electrostatic charges, the peptide content here refers to the manufacturer's specification (r-Peptide) of 1 mg Aβ per vial.

Each of the Aβ aliquots was measured 5 times, the protein aliquots 2 times.

Table 27: Determined peptide content of the different standards (species-specific ID)

Peptide content [%]		
Myoglobin (95-100%)	96.44 ± 3.32	n = 6
Myoglobin (≥98%, SDS-PAGE)	100.72 ± 2.84	n = 6
Lysozyme (≥90%)	97.44 ± 0.89	n = 6
Lysozyme (VETRANAL)	99.98 ± 1.57	n = 6
Amyloid β 1-40 (98%)	126.78 ± 0.05	n = 15
Amyloid β 1-42 (>97%)	52.56 ± 0.01	n = 15

The values obtained for the proteins are in good agreement with the information provided by the manufacturers. The peptide content of Aβ, however, deviates much from the specifications. Aβ40 showed values that were more than 2.4 times higher than Aβ42. External Calibration and on-line ID also showed similar ratios between the two peptides.

Since the entire content of the vial has been solved and the differences between the individual fractions are small, it is to be assumed that there is a problem with the weight specifications of the manufacturer.

In another attempt, where a different vial of Aβ was used, Aβ40 was weighed in completely and the microbalance showed a value of 1.268 mg, which fits well with the obtained peptide content of 126.78%. Unfortunately, negative values were noted for Aβ42, as it has been floating in the air when weighed due to electrostatic charges.

Based on these facts, r-Peptide was asked about their weighing methods. According to them no balance was used, nor do they recommend the use of one. Instead they prepare a solution of the peptide, analyse it chromatographically by means of amino acid analysis, and lyophilize the required amount in the vial. In addition, 5-10% more of the product are added to compensate for potential losses during resuspension of the peptide. This statement could provide a good explanation for the results. With the procedure described by the manufacturer, many errors in the determination of the peptide content are possible. In contrast to simple weighing, an amino acid analysis has numerous influencing factors, such as calibration, measuring conditions or evaluation,

resulting in greater uncertainty. In addition to possible losses during lyophilization, the supplement of another 5-10% product makes it impossible to estimate the exact peptide content, so it is misleading to state 1 mg on the analysis certificate.

3.5 Characterization of the standards using size exclusion chromatography

To ensure consistent performance of the method, a protein mix containing human serum albumin, myoglobin, glutathione disulfide and methionine was measured several times. As can be seen in **Figure 36**, all components could be successfully separated within 8 min.

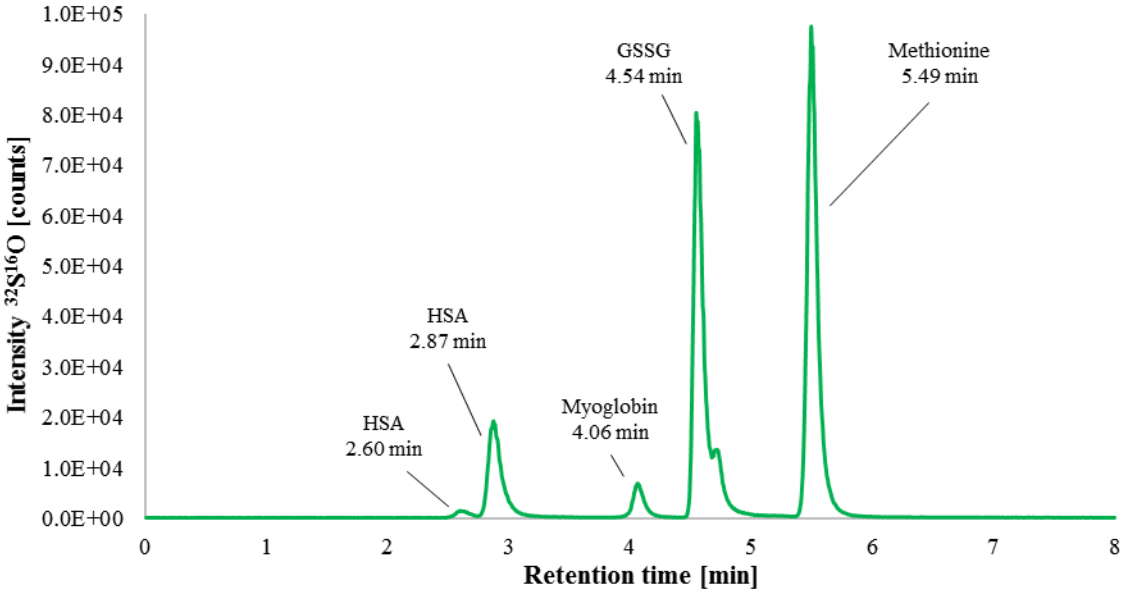

Figure 36: Chromatogram of a protein mix containing HSA, myoglobin, GSSG and methionine (50 mg L^{-1})

Due to the low mass of both Aβ peptides (4.3 and 4.5 kDa), a peak in the range of GSSG was to be expected. At 4.69 min, this peak was visible. Unfortunately, however, the peptides appear to have partially degraded in the solution (1% NH_4OH). In the low molecular weight region, there are several broad peaks, most likely from degradation products such as methionine, cysteine or sulfate.

In order to confirm this, 3 individually stored fractions of both peptides were measured, whereby the same peak pattern could be found again. This is most likely a consequence of the long storage time of 2-3 weeks in solution, because according to the manufacturer the peptides are only stable for 1-2 weeks at -80°C unless they are lyophilized again. Unfortunately, compliance with this timeframe was not possible due to technical issues.

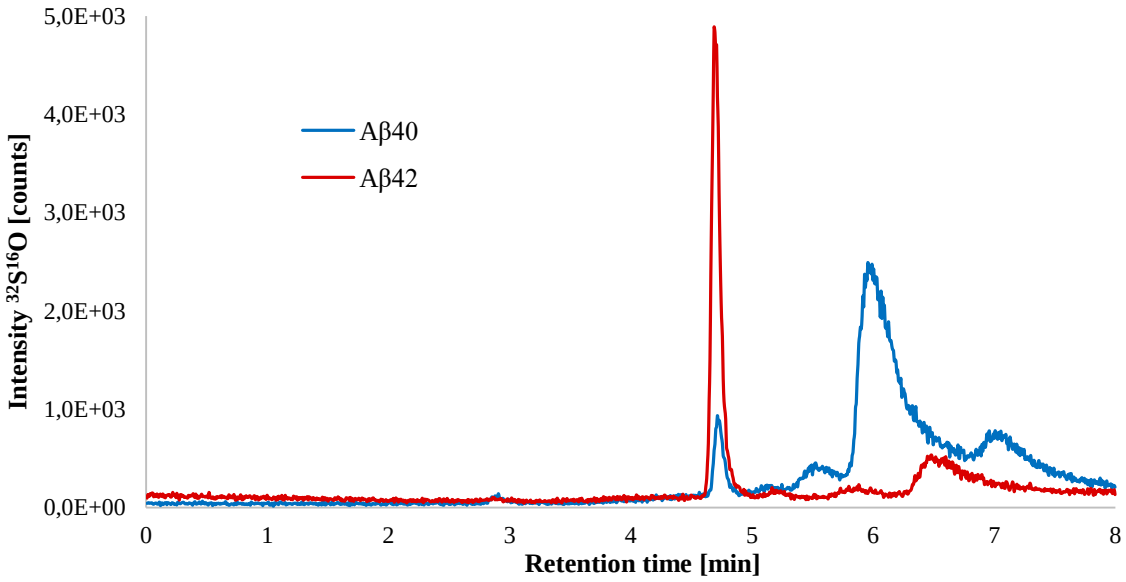

Figure 37: Comparison of the chromatograms of Aβ40 and Aβ42 at similar concentration (~ 100 mg L^{-1})

Interestingly, there were also large differences between the two peptides. While in Aβ42 59% of the signal belongs to the peptide, in Aβ40 it is only 5%, which shows significant instability of Aβ40. In addition, despite the same concentration, the area of Aβ40 was 2.38 times greater than that of Aβ42, which is in good agreement with the results of the species-specific IDMS.

Despite the decomposition of the peptides, it can be assumed from the chromatogram that the purity is relatively high, since no peak was seen in the high-molecular range.

Compared to the small peptides, the proteins showed significantly higher stability under the same conditions, since no LMW peaks were seen.

Typical for myoglobin are two peaks at 3.58 and 4.06 min, representing the substance and its dimer, which can be found in small quantities. Both peaks are visible in the standards, but also a third one at 4.72 min. While it only accounts for 2.6% of the area in myoglobin (≥98%), it is more pronounced in the myoglobin (95-100%) with 41%. Since the more impure myoglobin has been in use for a few years, there is a possibility that myoglobin eventually degrades to a smaller peptide or protein with time, since amino acids or sulfate are excluded due to the retention time. One possibility for this would be for the heme, which is noncovalently bound to the nitrogen atoms of myoglobin's histidines (**Figure 39**), to cleave, causing about 600 Da mass to be lost, resulting in

a retention shift. The split heme would not be visible in the chromatogram, since it has no sulfur atoms. [84]

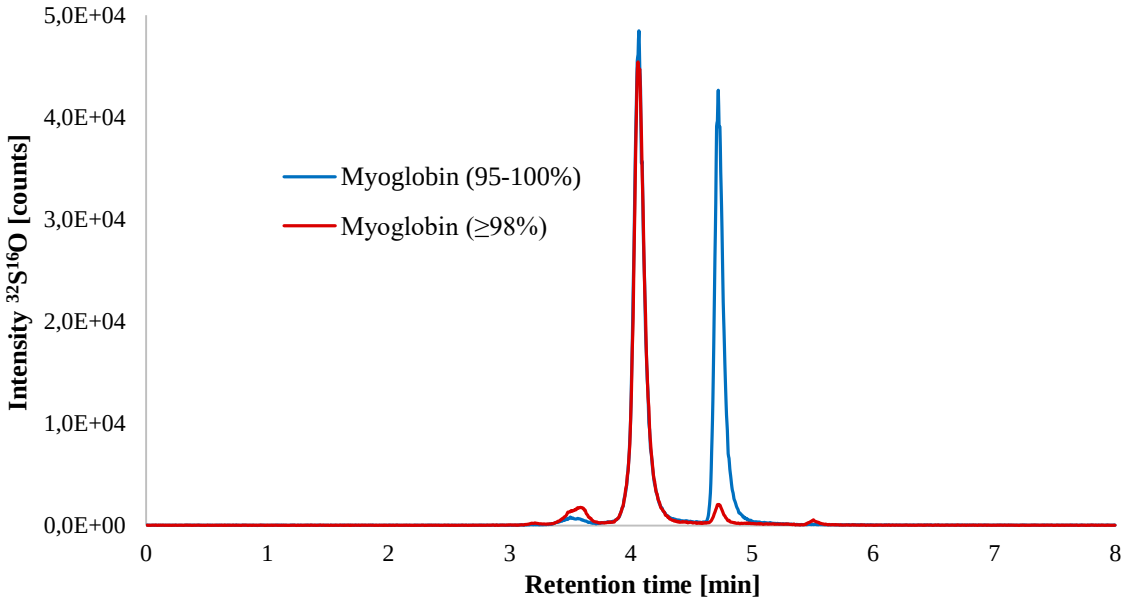

Figure 38: Comparison of the chromatograms between the different purity grades of myoglobin (500 mg L^{-1})

In any case, it was possible to confirm the purity of myoglobin (≥98%), since 97.4% of the peptide content belonged to myoglobin and its dimer in the SEC measurement.

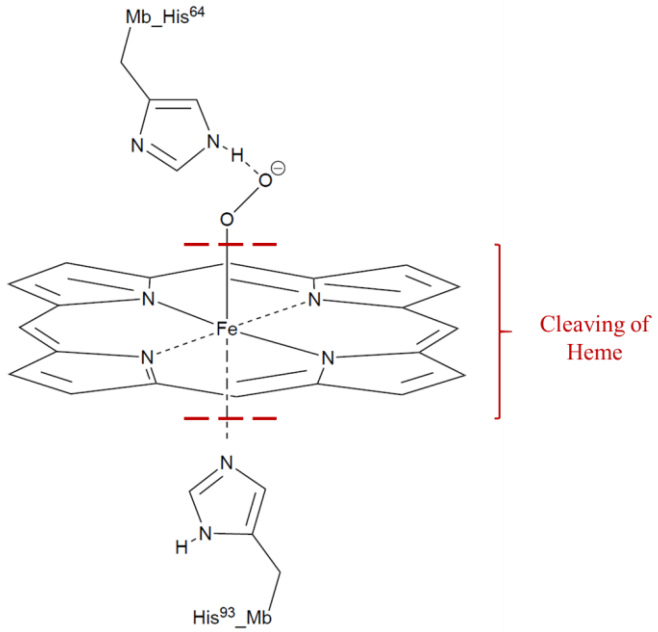

Figure 39: Non covalent binding of heme to the histidine of myoglobin [85]

The lysozyme standards, on the other hand, showed two peaks that overlap with each other in a characteristic pattern, so it can be assumed that this is not a contamination. Despite having similar mass as myoglobin (14.3 kDa), lysozyme showed a significantly longer retention time of 5.18 min, which is why it can be assumed that the protein in solution has a relatively low hydrodynamic volume.

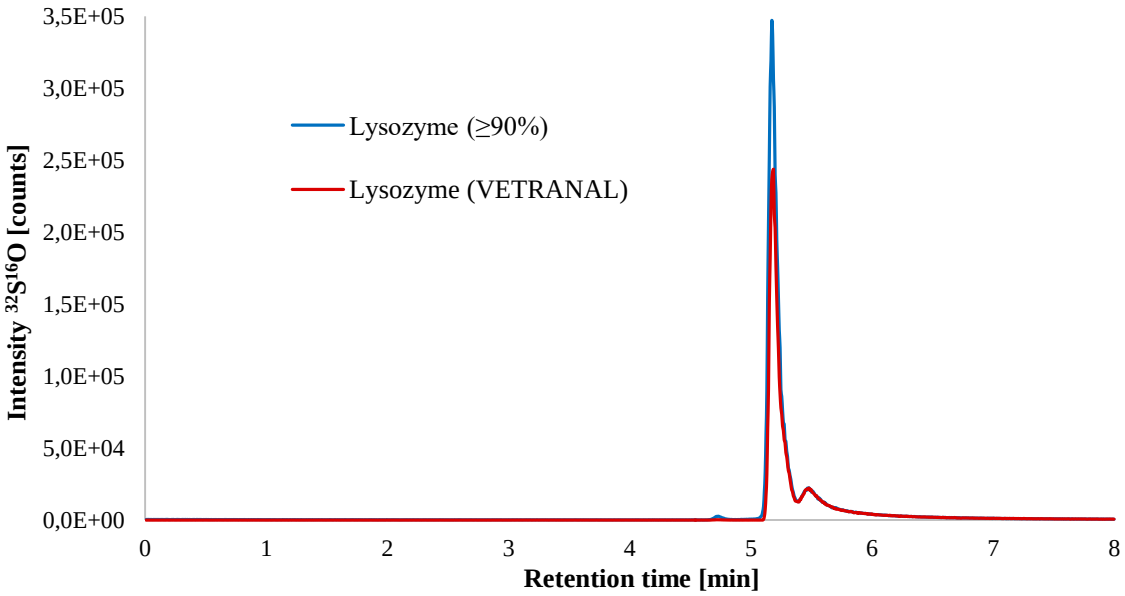

Figure 40: Comparison of the chromatograms between the different purity grades of lysozyme (500 mg L^{-1})

The only other peak was found at 4.72 min, as in myoglobin, but in much smaller amounts, which is why 99.5% of the area belonged to the protein in the case of lysozyme (≥90%) and 99.9% to lysozyme (VETRANAL), confirming their purity.

4. Conclusion

This work successfully demonstrated the capabilities of species-specific isotope dilution in combination with HPLC-ICP-MS/MS to determine the peptide content and thus the purity in protein standards.

The sample preparation with performic acid led to almost complete hydrolysis and oxidation of the proteins, with only small amounts of the unoxidized forms remaining. The choice of the evaporation system played a crucial role in the stability of the amino acids.

The best way to ensure the chromatographic separation of the amino acids was via an anion exchange column with NH_4Ac gradient. Reversed phase was not able to differentiate the oxidized forms. Regular cleaning of the column with the prescribed washing solution (80% ACN, 200mM HCl) was important to keep the sulfur background to a minimum. Contaminations of the injection needle could also be removed using 20% MeOH.

Species-specific isotope dilution using an ^{34}S-enriched yeast hydrolysate has proven to be suitable for determining the peptide content in an accurate manner, since in contrast to external calibration or on-line isotope dilution, errors in sample preparation are compensated for. This was also confirmed by multiple measurements of the standard reference material NIST 2389a. By applying this method to commercially available protein standards (myoglobin, lysozyme) with different purity grades, measurements were successfully tested.

When measuring the β-amyloid standards, however, it was found that the peptide content differed significantly from the information provided by the manufacturer. It was particularly noticeable that Aβ40 had a significantly higher content compared to Aβ42, which could be observed in numerous measurements.

Finally, size-exclusion ICP-MS/MS should reveal impurities in the peptides. However, this was not possible for Aβ because, unlike the other protein standards, it quickly disintegrated despite correct storage at -90°C. Aβ40 was particularly affected, while Aβ42 remained relatively stable.

However, it seems unlikely that there is a purity problem of the peptides, but much more an error in the manufacturing process. Small peptides such as Aβ can hardly be weighed in due to electrostatic interactions, which is why the manufacturer has resorted to other methods. Peptide

solutions are determined chromatographically, and corresponding amounts are lyophilized in the vial, with additional amounts added to compensate for losses during dissolving. Thus, it can never be guaranteed that an exact amount of the peptide will be in the vial.

Based on these findings, the investigated β-amyloid standards should not be used for clinical analysis in their current state, since the irregularities in the peptide content can have a significant impact on important medical decisions.

Literature

1. Fallon, C.K., *Chronic Disease in the Twentieth Century: A History: Aging Bones: A Short History of Osteoporosis.* Journal of the History of Medicine and Allied Sciences, 2016. **71**(2): p. 238-242.
2. Bateman, R.J., et al., *Clinical and Biomarker Changes in Dominantly Inherited Alzheimer's Disease.* New England Journal of Medicine, 2012. **367**(9): p. 795-804.
3. *Global Health Estimates 2016: Deaths by Cause, Age, Sex, by Country and by Region, 2000-2016. Geneva, World Health Organization; 2018.*; Available from: https://www.who.int/healthinfo/global_burden_disease/en/.
4. *Role of metals and metal containing biomolecules in neurodegenerative diseases such as Alzheimer's disease, European Metrology Programme for Innovation and Research, 2016*. Available from: https://www.ptb.de/empir/remind-project.html.
5. Chu, L.W., *Alzheimer's disease: early diagnosis and treatment.* Hong Kong Med J, 2012. **18**(3): p. 228-37.
6. Enz, A. and P. Floersheim, *Cholinesterase Inhibitors: An Overview of their Mechanisms of Action*, in *Alzheimer Disease: From Molecular Biology to Theraphy*, R.E. Becker, et al., Editors. 1997, Birkhäuser Boston: Boston, MA. p. 211-215.
7. Welsh-Bohmer, K.A., *Defining "prodromal" Alzheimer's disease, frontotemporal dementia, and Lewy body dementia: are we there yet?* Neuropsychology review, 2008. **18**(1): p. 70-72.
8. Kollhoff, A.L., J.C. Howell, and W.T. Hu, *Automation vs. Experience: Measuring Alzheimer's Beta-Amyloid 1–42 Peptide in the CSF*. Frontiers in Aging Neuroscience, 2018. **10**(253).
9. Nussbaum, R.L. and C.E. Ellis, *Alzheimer's Disease and Parkinson's Disease.* New England Journal of Medicine, 2003. **348**(14): p. 1356-1364.
10. *2015 Alzheimer's disease facts and figures.* Alzheimer's & Dementia: The Journal of the Alzheimer's Association, 2015. **11**(3): p. 332-384.
11. Bature, F., et al., *Signs and symptoms preceding the diagnosis of Alzheimer's disease: a systematic scoping review of literature from 1937 to 2016.* BMJ Open, 2017. **7**(8): p. e015746.

12. Goldsworthy, M.R. and A.-M. Vallence, *The Role of β-Amyloid in Alzheimer's Disease-Related Neurodegeneration.* The Journal of Neuroscience, 2013. **33**(32): p. 12910-12911.
13. Brothers, H.M., M.L. Gosztyla, and S.R. Robinson, *The Physiological Roles of Amyloid-β Peptide Hint at New Ways to Treat Alzheimer's Disease.* Frontiers in Aging Neuroscience, 2018. **10**(118).
14. Pawlowski, M., S.G. Meuth, and T. Duning, *Cerebrospinal Fluid Biomarkers in Alzheimer's Disease-From Brain Starch to Bench and Bedside.* Diagnostics (Basel, Switzerland), 2017. **7**(3): p. 42.
15. Yoon, S.-S. and S.A. Jo, *Mechanisms of Amyloid-β Peptide Clearance: Potential Therapeutic Targets for Alzheimer's Disease.* Biomolecules & therapeutics, 2012. **20**(3): p. 245-255.
16. Pearson, H.A. and C. Peers, *Physiological roles for amyloid beta peptides.* The Journal of physiology, 2006. **575**(Pt 1): p. 5-10.
17. Das, B., S. Dasgupta, and S. Ray, *Potential therapeutic roles of retinoids for prevention of neuroinflammation and neurodegeneration in Alzheimer’s disease.* Neural Regeneration Research, 2019. **14**(11): p. 1880-1892.
18. Khondker, A., R.J. Alsop, and M.C. Rheinstädter, *Membrane-Accelerated Amyloid-β Aggregation and Formation of Cross-β Sheets.* Membranes, 2017. **7**(3): p. 49.
19. Rakez Kayed, C.A.L.-R., *Molecular Mechanisms of Amyloid Oligomers Toxicity.* Journal of Alzheimer's Disease, 2012. **33** p. 67-78.
20. Faller, P. and C. Hureau, *Bioinorganic chemistry of copper and zinc ions coordinated to amyloid-β peptide.* Dalton Transactions, 2009(7): p. 1080-1094.
21. Cheignon, C., et al., *Identification of key structural features of the elusive Cu–Aβ complex that generates ROS in Alzheimer's disease.* Chemical Science, 2017. **8**(7): p. 5107-5118.
22. Roberts, B.R., et al., *The role of metallobiology and amyloid-β peptides in Alzheimer's disease.* Journal of Neurochemistry, 2012. **120**(s1): p. 149-166.
23. By M. del C. Cárdenas-Aguayo, M.d.C.S.-L., M. Cortes-Ortiz, B. Jiménez-Ramos, L. Gómez-Virgilio, G. Ramírez-Rodríguez, E. Vera- Arroyo, R. Fiorentino-Pérez, U. García, J. Luna-Muñoz and M.A. Meraz-Ríos, *Physiological Role of Amyloid Beta in Neural Cells: The Cellular Trophic Activity.* Neurochemistry, 2013.

24. Giuffrida, M.L., et al., *The Monomer State of Beta-Amyloid: Where the Alzheimer's Disease Protein Meets Physiology*, in *Reviews in the Neurosciences*. 2010. p. 83.
25. Blennow, K. and H. Zetterberg, *Biomarkers for Alzheimer's disease: current status and prospects for the future.* Journal of Internal Medicine, 2018. **284**(6): p. 643-663.
26. Bature, F., et al., *Signs and symptoms preceding the diagnosis of Alzheimer's disease: a systematic scoping review of literature from 1937 to 2016.* BMJ open, 2017. **7**(8): p. e015746-e015746.
27. Niemantsverdriet, E., et al., *Alzheimer's disease CSF biomarkers: clinical indications and rational use.* Acta neurologica Belgica, 2017. **117**(3): p. 591-602.
28. Menéndez-González, M., *Routine lumbar puncture for the early diagnosis of Alzheimer's disease. Is it safe?* Frontiers in aging neuroscience, 2014. **6**: p. 65-65.
29. Kim, Y., P. Rosenberg, and E. Oh, *A Review of Diagnostic Impact of Amyloid Positron Emission Tomography Imaging in Clinical Practice.* Dementia and Geriatric Cognitive Disorders, 2018. **46**(3-4): p. 154-167.
30. Moghbel, M., A. Newberg, and A. Alavi, *Chapter 12 - Positron emission tomography: ligand imaging*, in *Handbook of Clinical Neurology*, J.C. Masdeu and R.G. González, Editors. 2016, Elsevier. p. 229-240.
31. Palmqvist, S., et al., *Cerebrospinal fluid analysis detects cerebral amyloid-β accumulation earlier than positron emission tomography.* Brain : a journal of neurology, 2016. **139**(Pt 4): p. 1226-1236.
32. Gomperts, S.N., et al., *Imaging amyloid deposition in Lewy body diseases.* Neurology, 2008. **71**(12): p. 903-910.
33. Sharma, N. and A.N. Singh, *Exploring Biomarkers for Alzheimer's Disease.* Journal of clinical and diagnostic research : JCDR, 2016. **10**(7): p. KE01-KE6.
34. Thomann, P.A., et al., *Association of total tau and phosphorylated tau 181 protein levels in cerebrospinal fluid with cerebral atrophy in mild cognitive impairment and Alzheimer disease.* Journal of psychiatry & neuroscience : JPN, 2009. **34**(2): p. 136-142.
35. Zetterberg, H. and J.M. Schott, *Biomarkers for Alzheimer's disease beyond amyloid and tau.* Nature Medicine, 2019. **25**(2): p. 201-203.

36. Shah, M. and J.A. Caruso, *Inductively coupled plasma mass spectrometry in separation techniques: Recent trends in phosphorus speciation.* Journal of Separation Science, 2005. **28**(15): p. 1969-1984.
37. Wilschefski, S.C. and M.R. Baxter, *Inductively Coupled Plasma Mass Spectrometry: Introduction to Analytical Aspects.* The Clinical biochemist. Reviews, 2019. **40**(3): p. 115-133.
38. Giné, M.F. and A.P. Packer, *Online isotope dilution and inductively coupled plasma mass spectrometry: from elemental to species quantification.* Journal of the Brazilian Chemical Society, 2010. **21**: p. 575-589.
39. Theiner, S., *Pharmacokinetic and bioimaging studies of platinumbased anticancer complexes by ICP-MS and LA-ICP-MS*. 2015, University of Vienna.
40. Chajduk, E. and H. Polkowska-Motrenko, *Application of ICP-MS, INAA and RNAA to the determination of some "difficult" elements in infant formulas.* Journal of radioanalytical and nuclear chemistry, 2017. **311**(2): p. 1347-1353.
41. Pröfrock, D. and A. Prange, *Inductively Coupled Plasma–Mass Spectrometry (ICP-MS) for Quantitative Analysis in Environmental and Life Sciences: A Review of Challenges, Solutions, and Trends.* Applied Spectroscopy, 2012. **66**(8): p. 843-868.
42. Thomas, R., *Practical Guide to ICP-MS. A Tutorial for Beginners.* 3rd ed. 2013: Boca Raton: CRC Press.
43. March, R.E. and J.F.J. Todd, *Radio frequency quadrupole technology: Evolution and contributions to mass spectrometry.* International Journal of Mass Spectrometry, 2015. **377**: p. 316-328.
44. Miller, P.E. and M.B. Denton, *The quadrupole mass filter: Basic operating concepts.* Journal of Chemical Education, 1986. **63**(7): p. 617.
45. Gross, J.H., *Massenspektrometrie. Ein Lehrbuch.* 2013: Springer Spektrum.
46. Vanhaecke, F., et al., *Precise Measurement of Isotope Ratios with a Double-Focusing Magnetic Sector ICP Mass Spectrometer.* Analytical Chemistry, 1996. **68**(3): p. 567-569.
47. Frimmel, F.H., *Analytische Chemie. Von Matthias Otto VCH Verlagsgesellschaft, Weinheim. 1995, ISBN 3-527-28691-8, 668 S., brosch., DM 68,–.* Acta hydrochimica et hydrobiologica, 1996. **24**(3): p. 152-152.

48. Holmes, J.L., *Metastable Ions*, in *Encyclopedia of Spectroscopy and Spectrometry*, J.C. Lindon, Editor. 1999, Elsevier: Oxford. p. 1291-1297.
49. Boesl, U., *Time-of-flight mass spectrometry: Introduction to the basics.* Mass Spectrometry Reviews, 2017. **36**(1): p. 86-109.
50. Theiner, S., *The use of strontium isotope ratio measurements by MC-ICP-MS for fundamental studies on diagenesis and for the reconstruction of animal migration at the Celtic excavation site Roseldorf.* 2011, University of Vienna.
51. Walczyk, T., *TIMS versus multicollector-ICP-MS: coexistence or struggle for survival?* Analytical and Bioanalytical Chemistry, 2004. **378**(2): p. 229-231.
52. Hsiung, C.-S., et al., *Minimizing interferences in the quantitative multielement analysis of trace elements in biological fluids by inductively coupled plasma mass spectrometry.* Clinical Chemistry, 1997. **43**(12): p. 2303-2311.
53. Machado, R.C., et al., *Complex samples and spectral interferences in ICP-MS: Evaluation of tandem mass spectrometry for interference-free determination of cadmium, tin and platinum group elements.* Microchemical Journal, 2017. **130**: p. 271-275.
54. D'Ilio, S., et al., *Dynamic reaction cell ICP-MS for determination of total As, Cr, Se and V in complex matrices: Still a challenge? A review.* Analytica Chimica Acta, 2011. **698**(1): p. 6-13.
55. Tanner, S.D., V.I. Baranov, and D.R. Bandura, *Reaction cells and collision cells for ICP-MS: a tutorial review.* Spectrochimica Acta Part B: Atomic Spectroscopy, 2002. **57**(9): p. 1361-1452.
56. Leonhard, P., *Entwicklung einer spurenanalytischen Methode zur direkten Bestimmung von Elementspuren in verdünntem Meerwasser mit Hilfe der induktiv gekoppelten Plasma Massenspektrometrie mit integrierter Reaktions-/Kollisionszelle*, in *Umweltwissenschaften* Universität Lüneburg
57. I. Baranov, V. and S. D. Tanner, *A dynamic reaction cell for inductively coupled plasma mass spectrometry (ICP-DRC-MS) . Part 1. The rf-field energy contribution in thermodynamics of ion-molecule reactions.* Journal of Analytical Atomic Spectrometry, 1999. **14**(8): p. 1133-1142.
58. Balcaen, L., et al., *Accurate determination of ultra-trace levels of Ti in blood serum using ICP-MS/MS.* Analytica Chimica Acta, 2014. **809**: p. 1-8.

59. Bolea-Fernandez, E., et al., *Overcoming spectral overlap via inductively coupled plasma-tandem mass spectrometry (ICP-MS/MS). A tutorial review.* Journal of Analytical Atomic Spectrometry, 2017. **32**(9): p. 1660-1679.
60. Balcaen, L., et al., *Accurate determination of S in organic matrices using isotope dilution ICP-MS/MS.* Journal of Analytical Atomic Spectrometry, 2013. **28**(1): p. 33-39.
61. Amais, R.S., et al., *Determination of P, S and Si in biodiesel, diesel and lubricating oil using ICP-MS/MS.* Analytical Methods, 2014. **6**(13): p. 4516-4520.
62. Møller, L.H., et al., *Quantification of pharmaceutical peptides in human plasma by LC-ICP-MS sulfur detection.* Journal of Analytical Atomic Spectrometry, 2016. **31**(9): p. 1877-1884.
63. Nordberg, M., J. Duffus, and D.M. Templeton, *Glossary of terms used in toxicokinetics (IUPAC Recommendations 2003),* in *Pure and Applied Chemistry*. 2004. p. 1033.
64. Feldmann, J., A. Raab, and E.M. Krupp, *Importance of ICPMS for speciation analysis is changing: future trends for targeted and non-targeted element speciation analysis.* Analytical and bioanalytical chemistry, 2018. **410**(3): p. 661-667.
65. Carneado, S., et al., *Mercury(ii) and methylmercury determination in water by liquid chromatography hyphenated to cold vapour atomic fluorescence spectrometry after online short-column preconcentration.* Analytical Methods, 2015. **7**(6): p. 2699-2706.
66. Raber, G., et al., *Quantitative speciation of arsenic compounds when using organic solvent gradients in HPLC-ICPMS.* Journal of Analytical Atomic Spectrometry, 2010. **25**(4): p. 570-576.
67. Gong, J., et al., *Developing ICP-MS/MS for the detection and determination of synthetic DNA-protein crosslink models via phosphorus and sulfur detection.* Analytical and bioanalytical chemistry, 2015. **407**(9): p. 2433-2437.
68. Boorn, A.W. and R.F. Browner, *Effects of organic solvents in inductively coupled plasma atomic emission spectrometry.* Analytical Chemistry, 1982. **54**(8): p. 1402-1410.
69. De Wolf, K., et al., *A comparison between HPLC-dynamic reaction cell-ICP-MS and HPLC-sector field-ICP-MS for the detection of glutathione-trapped reactive drug metabolites using clozapine as a model compound.* Journal of Analytical Atomic Spectrometry, 2010. **25**(3): p. 419-425.

70. Yu-Feng, L., et al., *Direct quantitative speciation of selenium in selenium-enriched yeast and yeast-based products by X-ray absorption spectroscopy confirmed by HPLC-ICP-MS.* Journal of Analytical Atomic Spectrometry, 2010. **25**(3): p. 426-430.
71. Jose Alonso, P.G., *Isotope Dilution Mass Spectrometry*. 2013: Royal Society of Chemistry.
72. Rodríguez-González, P. and J.I. García Alonso, *Recent advances in isotope dilution analysis for elemental speciation.* Journal of Analytical Atomic Spectrometry, 2010. **25**(3): p. 239-259.
73. Hermann, G., et al., *13C-labelled yeast as internal standard for LC–MS/MS and LC high resolution MS based amino acid quantification in human plasma.* Journal of Pharmaceutical and Biomedical Analysis, 2018. **155**: p. 329-334.
74. Bhowmik, S.K., et al., *Application of 13C isotope labeling using liquid chromatography mass spectrometry (LC-MS) to determining phosphate-containing metabolic incorporation.* Journal of Mass Spectrometry, 2013. **48**(12): p. 1270-1275.
75. Kleigrewe, K., et al., *New Approach via Gene Knockout and Single-Step Chemical Reaction for the Synthesis of Isotopically Labeled Fusarin C as an Internal Standard for the Analysis of this Fusarium Mycotoxin in Food and Feed Samples.* Journal of Agricultural and Food Chemistry, 2012. **60**(34): p. 8350-8355.
76. B'Hymer, C. and J.A. Caruso, *Selenium speciation analysis using inductively coupled plasma-mass spectrometry.* Journal of Chromatography A, 2006. **1114**(1): p. 1-20.
77. Hermann, G., et al., *In vivo synthesized 34S enriched amino acid standards for species specific isotope dilution of proteins.* Journal of Analytical Atomic Spectrometry, 2016. **31**(9): p. 1830-1835.
78. Rampler, E., et al., *LILY-lipidome isotope labeling of yeast: in vivo synthesis of 13C labeled reference lipids for quantification by mass spectrometry.* Analyst, 2017. **142**(11): p. 1891-1899.
79. *SelectScience. Eppendorf New Brunswick™ BioFlo® 310.* https://www.selectscience.net/images/products/6487_BioFlo-310.jpg.ashx?width=250&height=250&bgcolor=white.
80. Bamonti, L., et al., *Accurate high throughput quantification of selenium in biological samples – the potential of combining isotope dilution ICP-tandem mass spectrometry with flow injection.* Journal of Analytical Atomic Spectrometry, 2016. **31**(11): p. 2227-2232.

81. Swart, C., O. Rienitz, and D. Schiel, *Impact of pump flow fluctuations on post column online ID-ICP-MS.* Analytical and Bioanalytical Chemistry, 2011. **401**(6): p. 2025.

82. Naoki Sugiyama, K.N., *Reaction data for 70 elements using O_2, NH_3 and H_2 gases with the Agilent 8800 Triple Quadrupole ICP-MS*. 2014, Agilent Technologies.

83. Zhao, G. and E. London, *An amino acid "transmembrane tendency" scale that approaches the theoretical limit to accuracy for prediction of transmembrane helices: Relationship to biological hydrophobicity.* Protein Science, 2006. **15**(8): p. 1987-2001.

84. Li, Y.-T., et al., *Studies on heme binding in myoglobin, hemoglobin, and cytochrome c by ion spray mass spectrometry.* Journal of the American Society for Mass Spectrometry, 1993. **4**(8): p. 631-637.

85. Møller, J.K.S. and L.H. Skibsted, *Myoglobins: the link between discoloration and lipid oxidation in muscle and meat.* Química Nova, 2006. **29**: p. 1270-1278.

List of tables

List of figures